Research Square

Preprints are preliminary reports that have not undergone peer review. They should not be considered conclusive, used to inform clinical practice, or referenced by the media as validated information.

TMEM119+ microglia MHC class I restricted antigen presentation impacts CD8 T cell memory, effector status, and blood-brain barrier disruption during neurotropic virus infection

Aaron Johnson

johnson.aaron2@mayo.edu

Mayo Clinic

Marina Seady

Mayo Clinic

Mark Maynes

Department of Immunology, Mayo Clinic College of Medicine and Science

Javonte Thelwell

Mayo Clinic

Fang Jin

Mayo Clinic

Michael Hansen

Mayo Clinic

Hadley Jensen

Mayo Clinic https://orcid.org/0009-0000-4651-8807

Ryann Witter

Mayo Clinic

Carley Owens

Mayo Clinic

Asma Hassani

Mayo Clinic https://orcid.org/0000-0001-7792-2140

Cody Lewis

Mayo Clinic

Michael Forston

Mayo Clinic https://orcid.org/0000-0001-7759-225X

Article

Keywords: Microglia, antigen presentation, CD8 T cells, perforin, MHC class I

Posted Date: June 24th, 2026

DOI: https://doi.org/10.21203/rs.3.rs-10061124/v1

License: This work is licensed under a Creative Commons Attribution 4.0 International License.
Read Full License

Additional Declarations: There is **NO** Competing Interest.

TMEM119+ microglia MHC class I restricted antigen presentation impacts CD8 T cell memory, effector status, and blood-brain barrier disruption during neurotropic virus infection

Author list: Marina Seady[1], Mark A. Maynes[1,2], Javonte S. Thelwell[2], Fang Jin[1], Michael J. Hansen[1], Hadley E. Jensen[1], Ryann K. Witter[1], Carley A. Owens[1], Asma Hassani[1], Cody L. Lewis[1,2], Michael D. Forston[1], Aaron J. Johnson[1,3,4]*

[1]Mayo Clinic Department of Immunology, Rochester, MN

[2]Graduate School of Biomedical Sciences, Mayo Clinic, Rochester, MN

[3]Mayo Clinic Department of Neurology, Rochester, MN

[4]Mayo Clinic Department of Molecular Medicine, Rochester, MN

*Correspondence
Aaron J. Johnson
Johnson.aaron2@mayo.edu

Keywords: Microglia, antigen presentation, CD8 T cells, perforin, MHC class I

16 **Graphical abstract:**

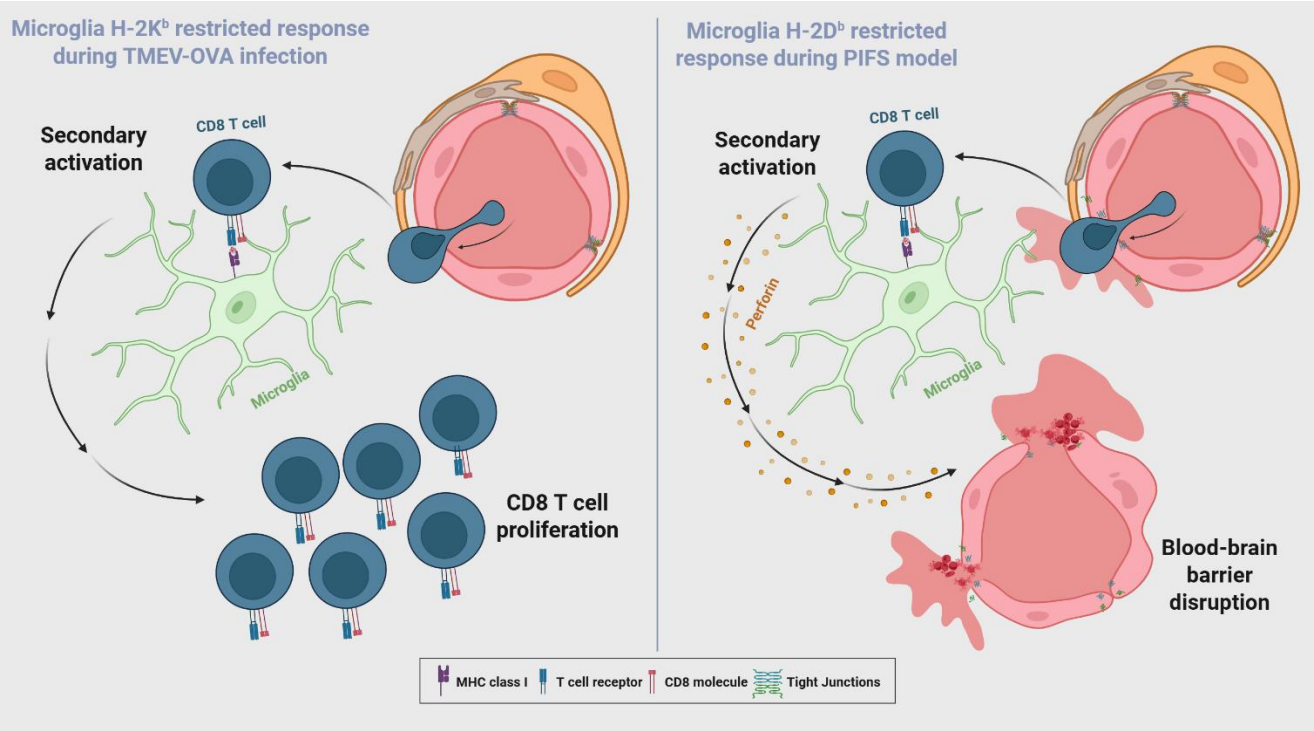

17

Abstract:

The impact of microglia antigen presentation on CNS infiltrating CD8 T cells responses during neurotropic virus infection remains undefined. Using Theiler's murine encephalomyelitis virus (TMEV) infection of neurons as a model system, we generated H-2K^b and H-2D^b Tmem119 conditional knockout mice. During TMEV infection, we determined using Tmem119 K^b cKO mice that microglia H-2K^b contributes to antiviral CD8 T cell proliferation in the brain. Meanwhile, using Tmem119 D^b cKO mice we determined that microglia H-2D^b increased antiviral CD8 T cell perforin levels and the capacity to induce blood-brain barrier (BBB) disruption. Furthermore, microglial H-2D^b was essential for antigen-specific reactivation of CD8 tissue resident memory (TRM) cell recall responses and BBB disruption long after virus had been cleared. These findings demonstrate discrete roles of individual MHC class I genes on microglia in CD8 T cell proliferation, effector functions, memory recall and neuropathology.

31 **Introduction**

32 Neurotropic viral infections are responsible for acute and long-lasting neurological
33 manifestations, resulting in burdens on healthcare systems worldwide [1, 2]. The
34 contribution of long-lived memory T cells in the CNS well after viruses are cleared also
35 contribute to chronic neuroinflammation through means poorly understood [3, 4, 5, 6, 7].
36 Central to chronic neuroinflammation is microglial activation, which in turn modifies T cell
37 responses against neurotropic viruses [8, 9]. Microglia have the capacity to influence
38 neurotropic virus infections through the upregulation of phagocytosis machinery,
39 enhanced expression of proinflammatory molecules, and uptake of cellular debris [10, 11].
40 However, the role of microglia activation is not limited to innate immune function due to
41 their increased expression of antigen processing and presentation molecules [8, 12, 13, 14, 15].
42 As such, it is assumed microglia become fully competent antigen presenting cells which
43 boost antiviral T cell responses in the brain [8, 12, 13, 15]. However, it remains unclear how T
44 cell responses are altered acutely and long term when microglia are not directly infected
45 with virus [16].

46 Theiler's murine encephalomyelitis virus (TMEV) provides a neurotropic virus infection
47 model in which the contribution of discrete MHC class I molecules are well defined [17, 18,
48 19]. H-2D^b restricted, but not H-2K^b restricted CD8 T cells are required for viral clearance,
49 demonstrating the role of discrete MHC class I alleles [17]. To define how myeloid cells
50 impact T cell responses against neurotropic virus infection through H-2K^b and H-2D^b,
51 Goddery *et al*. evaluated the impact of conditionally deleting discrete MHC class I
52 molecules in CX3CR1+ cells following Theiler's murine encephalomyelitis virus (TMEV)
53 infection [8]. This conditional silencing of MHC class I restricted antigen presentation

54 resulted in a dampened CD8 T cell response and reduced brain atrophy post TMEV
55 infection [8]. In agreement with these findings, Moseman *et al.* analyzed vesicular stomatitis
56 virus (VSV) infection using a tracer for olfactory sensory neurons (OSNs) in the olfactory
57 bulb [15]. 6 days post VSV infection, fragments of labeled OSNs were found within
58 CX3CR1+ cells, also demonstrating in principle that microglia could acquire and present
59 antigen from virus-infected neurons [15].

60 In both of these studies, myeloid cells were determined to impact CD8 T cell responses,
61 potentially through the cross-presentation of virus antigen. However, it has remained
62 difficult to define the extent microglia enhance CD8 T cell responses in the brain through
63 MHC class I restricted antigen presentation due to the lack of microglia-specific tools.
64 Approaches using CX3CR1 Cre mice and cell depletion strategies targeting the colony-
65 stimulating factor 1 receptor (CSF1R) have been informative, but perivascular
66 macrophages and infiltrating myeloid cells are common off target effects of myeloid cell
67 ablation strategies that need consideration when interpreting results [20, 21, 22].

68 Using a novel single MHC class I Cre Lox approach developed by our laboratory in which
69 H-2D^b and H-2K^b can be deactivated in TMEM119+ cells, we sought to understand the
70 impact of microglia MHC class I restricted antigen presentation on acute antiviral CD8 T
71 cell responses and long lived CD8 T resident memory cells post virus clearance. Using
72 TMEV and recombinant TMEV encoding the model OVA (TMEV-OVA) antigen, we were
73 able to analyze virus antigen-specific CD8 T cells restricted to D^b class I and K^b class I
74 molecules, respectively. Our data supports that K^b and D^b have discrete roles in modifying
75 brain infiltrating CD8 T cells, and D^b restricted antigen presentation on microglia is

76 essential for CD8 tissue resident memory (TRM) recall. We also put forward evidence
77 that microglia antigen presentation promotes CD8 T cell induced BBB disruption.

78 **Methods**

79 *Animals*

80 Male and female C57BL/6J wildtype (WT) (stock no. 000664) and Tmem119-creER^{T2}
81 mice (stock no. 031820) were purchased from The Jackson Laboratory. H-2K^{b} LoxP and
82 H-2D^{b} LoxP mice were generated by our program, as previously described, in the
83 C57BL/6 background. H-2K^{b} LoxP and H-2D^{b} LoxP mice were crossed with Tmem119-
84 Cre^{ERT2} mice to generate Tmem119 K^{b} cKO and Tmem119 D^{b} cKO mice that express
85 Cre under the Tmem119 promoter and undergo microglia-specific targeted gene deletion
86 of H-2K^{b} and H-2D^{b} molecules. Mice were bred and maintained under specific pathogen-
87 free conditions at the Mayo Clinic Animal Facility. In the studies, 10–15-week-old mice
88 were used for all experiments with appropriate age- and sex-matched controls. All
89 experiments were conducted in accordance with guidelines from the National Institutes
90 of Health and with the approval of the Mayo Clinic Institutional Animal Care and Use
91 Committee.

92 *Tamoxifen administration*

93 Tamoxifen (Sigma-Aldrich, St. Louis, MO) was administered in corn oil (Sigma-Aldrich,
94 St. Louis, MO) at a concentration of 20mg/mL. Tamoxifen was dissolved in corn oil by
95 constant agitation overnight at 37°C in the dark. Tmem119 K^{b} cKO mice were
96 administered 75 mg/kg tamoxifen intraperitoneally at 8 weeks of age once a day for five
97 consecutive days using a 26-gauge 3/8” beveled needle. Tmem119 D^{b} cKO were

98 administered 75 mg/kg tamoxifen intraperitoneally at 8 weeks of age for 5 consecutive
99 days followed by one week of recovery without injections, and additional 5 days of
100 tamoxifen injections daily. The differential tamoxifen regime was defined after testing for
101 the expression of MHC class I molecules on TMEM119+ microglia after 1 week of
102 injections (sufficient for Tmem K^b cKO mice) or 2 weeks of injections (sufficient for
103 Tmem119 D^b cKO mice). Post tamoxifen recovery times of 1 week was incorporated prior
104 to experimental use of mice in experiments.

105 *TMEV and TMEV-OVA infection*

106 The Daniel's strain of Theiler's murine encephalomyelitis (TMEV) was prepared as
107 previously described [19]. TMEV-XhoI-OVA8 [TMEV-ovalbumin (OVA)] was generated and
108 prepared by our group, as previously described [23]. At 10–12 weeks of age, mice were
109 anaesthetized with 1–2% isoflurane and infected intracranially with 2×10^6 PFU (10 µl) of
110 the Daniel's strain of TMEV or 2×10^5 PFU of TMEV-OVA. Virus was delivered to the
111 right hemisphere of the brain via automatic 1 mL Hamilton syringe (Hamilton). Mice were
112 euthanized for high-dimensional flow cytometry of tissues at 7 days post-infection (dpi) or
113 according to experimental design displayed in every figure.

114 *FTY720 treatment and Bromodeoxyuridine (BrdU) administration*

115 FTY720 (Sigma, SML0700–5mg) was diluted to 0.15mg/mL in water such that a 100µL
116 intraperitoneal injection would be the equivalent of a 0.5mg/kg dose assuming a 30g
117 mouse. FTY720 was administered in this way twice a day over the course of appropriate
118 experiments to randomized, age matched Tmem119 K^b cKO and Cre negative littermate
119 controls. 100µL of 10mg/mL BrdU (BD Pharmingen, Cat #51–2420KC) solution was

120 administered intraperitoneally 5 days post intracranial TMEV-OVA infection. For BrdU
121 staining, manufacturer's instructions were followed according to the kit.

122 *Intravascular labeling*

123 For Intravascular labeling experiments, 200μL total volume (3μg of FITC αCD45 (Cat
124 #FITC 35–0451-U100, Tonbo) diluted in PBS) was injected into the tail vein 24 hours
125 before euthanasia.

126 *FITC-albumin leakage assay*

127 Mice were intravenously injected with 100 μL of a solution containing 66 kDa FITC-
128 conjugated albumin diluted in PBS 1 h prior to euthanasia to visualize regions of blood–
129 brain barrier disruption and vascular leakage. Mice were not perfused before euthanasia.
130 Brains were paraformaldehyde-fixed for 48 h following mouse euthanasia. FITC-albumin
131 injected brains were embedded in 4% agarose and sliced with a vibratome. All brain slices
132 were mounted on microscope slides and stored at 4°C. Images were acquired using the
133 Echo Revolution microscope. Analysis was performed using whole-slice thresholding
134 followed by thresholding of the FITC channel acquired by ImageJ (National Institutes of
135 Health). Results are shown as % of FITC per total area.

136 *Reactivation of virus antigen-specific CD8 T cells through peptide injection*

137 Between 55-65 days post-TMEV infection, mice were intravenously injected with 0.1 mg
138 (from a solution of 1mg/ml in PBS) of $VP2_{121–130}$ (FHAGSLLVFM) or control E7
139 (RAHYNIVTF) peptide (GenScript, Piscataway, NJ, USA) into the tail vein. Both of these
140 peptides are MHC I (D^b) restricted.

141 *Single-cell suspension*

142 Mice were euthanized via isoflurane per institutional animal care and use committee
143 (IACUC) guidelines and transcardially perfused with ice-cold PBS. Perfused brains were
144 processed following a previously published protocol designed for enrichment of brain
145 infiltrating leukocytes using the Dounce homogenization method followed by 30–38%
146 Percoll (Cat# P1644–1L, Sigma, St. Louis, MO) gradient centrifugation. Thymus and
147 spleen samples were processed using mechanical disruption with the rough side of two
148 microscope slides through a 70 μM filter. Blood was collected (100 μL) into 1 ml heparin
149 (100 U/mL). Spleens underwent ammonium-chloride-potassium (ACK) RBC lysis for 3
150 min and blood samples for 1 min. All samples were filtered using 70 μM filters, and
151 resulting cells were counted on the hemocytometer (Hausser Scientific, Horsham, PA)
152 using trypan blue to exclude dead cells (Gibco, Gaithersburg, MD). Alive cells were then
153 stained and ran on a flow cytometer.

154 *Flow cytometry*

155 When applicable, samples were stained with 50 μL of a 1:50 dilution of D^b: $VP2_{121-130}$
156 APC-labeled tetramer or a 1:50 dilution of K^b: $OVA_{257-264}$ APC-labeled tetramer (NIH
157 Tetramer Core Facility, Emory University). For tetramer staining, we incubated cells with
158 only the tetramer for 30 minutes at room temp before proceeding with staining with
159 viability dye and the rest of antibodies. Zombie UV dye (Cat# 423108, Biolegend) was
160 used at a 1:1000 concentration to identify and exclude non-viable cells. The Zombie UV
161 dye was stained separately for 20 minutes at room temp and washed off before staining
162 with the rest of the master mix. The following antibodies were used at a 1:50 dilution: PE-
163 Cy7 Tmem119 (ThermoFisher, Cat# 25-6119-82), BV510 CD4 (BioLegend, Cat#

164 100559), PE H-2K^b (BD Pharmingen, Cat# 5535570), PE H-2D^b (Biolegend, Cat#
165 111508), BV650 IFNγ (Biolegend, Cat# 505831), FITC perforin (Biolegend, Cat# 154310)
166 and Alexa Fluor 700 TNFα (Biolegend, Cat# 506338).The following antibodies were used
167 at a 1:100 dilution: BUV615 NK-1.1 (BD Biosciences, Cat# 751111), BUV395 F480 (BD
168 Horizon, Cat# 565614), BUV737 TCRβ (BD OptiBuild, Cat# 612821), BV421 CXCR3
169 (Biolegend, Cat# 1265522), BV570 CD44 (Biolegend, Cat# 103037), BV605 CD11C
170 (Biolegend, Cat# 117333), PerCP Ly6C (Biolegend, Cat# 128027), APC FIRE 750 CD62L
171 (Biolegend, Cat# 104450), APC FIRE 810 CD19 (Biolegend, Cat# 115578), BV421
172 CD103 (Biolegend, Cat#121422) and Pacific Blue CX3CR1 (Biolegend, Cat#149037).
173 The following antibodies were used at a 1:200 dilution: BV711 Ly-6G (BioLegend, Cat#
174 127643), Spark Blue 550 CD8a (BioLegend, Cat# 100780), BUV805 MHC II (BD
175 OptiBuild, Cat# 748844), BB700 CD24 (BD Biosciences, Cat# 746122) and Spark NIR
176 685 CD69 (Biolegend, Cat# 104558). The following antibodies were used at a
177 1:1000 dilution: PE-CF594 CD45 (BioLegend, Cat# 562420) and PE-Cy5 CD11b
178 (TONBO Biosciences, Cat# 55-0112-U100). To all master mixes of antibodies, FC block
179 (Cat# 553141, BD) was added at a 1:100 dilution to prevent non-specific binding. The
180 single-cell suspensions were next fixed and permeabilized with 250 µL of
181 Cytofix/Cytoperm fixation buffer (BD Biosciences, Franklin Lakes, NJ) for 20 min at
182 4 °C. Antibodies that tag intracellular proteins were used in a separate master mix, and
183 cells were stained after permeabilization. Across all staining conditions, cells were
184 analyzed on the spectral high parameter flow cytometer Cytek Aurora (Cytek, Fremont,
185 CA) and data was analyzed on FlowJo 10.1 (FlowJo LLC, Ashland, OR). High
186 dimensional analysis including UMAP analysis was also performed using FlowJo software

187 using DownSample and UMAP_R plugins. For BrdU staining, manufacturer's protocol
188 was followed.

189 *Parabiosis*

190 Two female age-matched mice of similar weight were selected. Mice were either
191 littermates or co-housed for a minimum of 2 weeks prior to surgery. Anesthesia was
192 induced and maintained with ketamine/xylazine (100/10 mg/kg; maintenance dose 30/3
193 mg/kg). Ophthalmic ointment was placed on eyes. Mice were tested for reflex responses
194 to ensure anesthetic depth. For analgesia during surgery, we administered intraperitoneal
195 carprofen and buprenorphine-SR subcutaneously (5 mg/kg and 1 mg/kg, respectively).
196 Animals were shaved on the flank and prepped for surgery with Betadine swabs and
197 sterile drapes. Using sharp scissors, a superficial epidermal incision was continuously
198 made along the flank starting at 0.5 cm rostral of olecranon to 0.5 cm superior to patella.
199 Skin absorbable 3–0 silk sutures were used to join elbow and knee joints (Ethicon Inc.).
200 Simple continuous suture was performed with absorbable 4–0 vicryl suture (Ethicon Inc.)
201 for closer of incision. Postoperatively, we administered 1 ml of 0.9% NaCl fluids
202 subcutaneously and analgesic carprofen intraperitoneally and buprenorphine-SR
203 subcutaneously. Mice were placed on heating pads and observed for a minimum of 3 h
204 after surgery. Prophylactically, mice were treated with antibiotic Enrofloxacin (50 mg/kg)
205 10 days postoperatively. Parabiont pairs underwent a minimum of 3 weeks of healing and
206 acclimation time before experimental use. The procedure was performed according to the
207 IACUC guidelines at Mayo Clinic.

208 *Magnetic Resonance imaging (MRI)*

MRI images were acquired and processed as previously described [24, 25]. A Bruker Avance II 300-MHZ (7T) vertical-bore small-animal animal system was used to conduct T1-weighted scans (Bruker Biospin, Billerica, MA, USA) following an intraperitoneal injection of gadolinium 15 minutes before the MRI. Anesthesia was induced with isoflurane and maintained for the duration of the scan. Respiratory rate and temperature were monitored. Analysis and quantification of the gadolinium leakage into the brain was performed using Analyze 12.0 software (Biomedical Imaging Resource, Mayo Clinic). The analysis of gadolinium leakage in the T1-weight MRIs was performed blinded.

Statistical analysis

When comparing results from two groups, an unpaired Student's t-test was used; when comparing results from two groups of paired mice, a paired Student's t-test was used; and when comparing results from three groups, a one-way ANOVA using Tukey's post hoc multiple comparisons test was used. A two-way ANOVA was used when comparing statistically significant differences between the means of three or more independent groups that had been split on two variables, using Šidák's test for multiple comparisons. All measurements in all experiments were taken from distinct samples. Normal distribution was tested using the Shapiro–Wilk test. All parabiont data employed pairwise comparisons. All statistical analyses were performed using Prism 10.0 (GraphPad Software), Excel or R. Data are presented as the mean ± standard deviation (SD), and all P-values are shown. Non-significant P-values ($P > 0.05$) are marked.

230 **Results**

231 **Establishment of microglia H-2K^b and H-2D^b conditional knockout (cKO) mice**

232 The challenge of dissecting microglial contributions to neurologic disease stems from the
233 use of strategies that also target additional myeloid cells, namely perivascular
234 macrophages, infiltrating monocytes, dendritic cells, macrophages and other circulating
235 myeloid cells [20, 22, 26]. Tmem119 expression is highly specific to microglia, enabling
236 targeted deletion employing Cre-Lox technologies in mouse models [27, 28]. Our laboratory
237 has developed tamoxifen-inducible conditional knockout strategies to dissect the
238 contribution of two discrete MHC class I molecules, H-2K^b and H-2D^b, on microglia. The
239 Tmem119 K^b cKO mice is designed to have H-2K^b ablation in microglia. Likewise,
240 Tmem119 D^b cKO mice is designed to have targeted inactivation of microglia H-2D^b
241 expression. Throughout this study, these mice with the ablation of K^b or D^b on TMEM119+
242 microglia will be compared to K^b Cre- littermate control or D^b Cre- littermate controls,
243 respectively. To confirm H-2K^b and H-2D^b expression was specifically ablated in
244 TMEM119+ microglia, we administered tamoxifen and then intracranially infected mice
245 with TMEV. Microglial expression of H-2K^b and H-2D^b in TMEM119+ cells in brains
246 isolated from TMEV infected animals was then assessed using spectral flow cytometry.
247 As intended, we observed a marked reduction of H-2K^b or H-2D^b in TMEM119+ cells in
248 these animals (Figure 1 A, C). To further validate specificity of MHC class I knockdown,
249 we assessed H-2K^b (Figure 1B) and H-2D^b (Figure 1D) expression in blood immune cell
250 populations and confirmed there was no difference between Cre- and Cre+ mice in both
251 K^b and D^b cKO mice.

252 We next wanted to determine if conditional deletion of K^b and D^b MHC class I molecules
253 on TMEM119+ cells impacted CD8 T cell development and repertoire diversity. We
254 analyzed TCR Vβ usage in the spleens of naïve animals for Tmem119 K^b cKO (Figure
255 1E) and Tmem119 D^b cKO mice (Figure 1F). We did not observe differences between
256 Tmem119 K^b and D^b cKO mice and Cre- littermate controls. As a measurement of
257 thymocyte output, we analyzed the percentages of single positive CD8 and CD4 T cells
258 for both cKOs (Figure 1G and 1H). We did not observe differences between groups,
259 demonstrating T cell development in the thymus is not affected by targeted ablation of
260 MHC class I molecules in microglia.

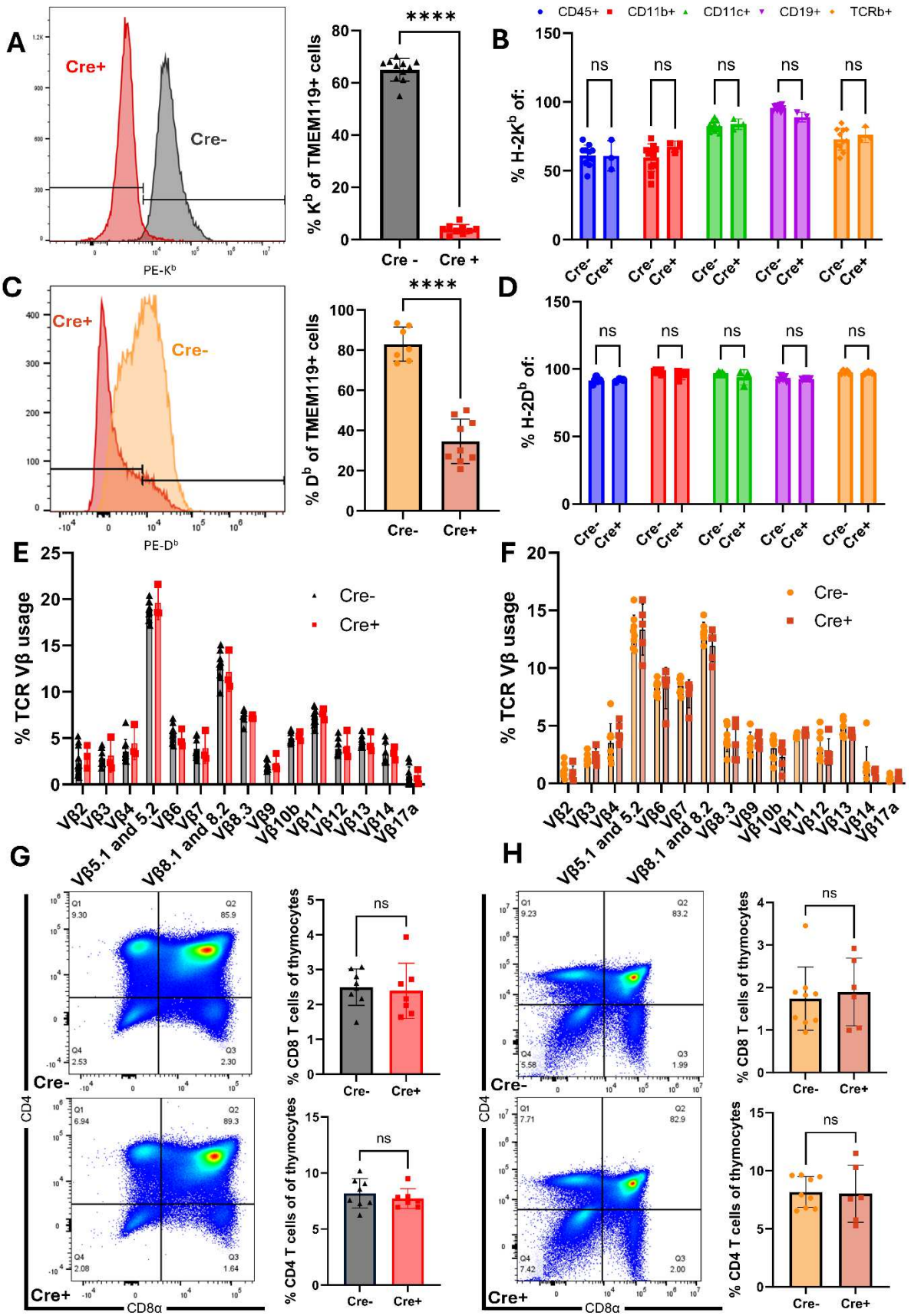
A
Cre+
Cre-
PE-Kᵇ
% Kᵇ of TMEM119+ cells
****
Cre -
Cre +
B
CD45+
CD11b+
CD11c+
CD19+
TCRb+
% H-2Kᵇ of:
ns
Cre-
Cre+
C
Cre+
Cre-
PE-Dᵇ
% Dᵇ of TMEM119+ cells
****
Cre-
Cre+
D
% H-2Dᵇ of:
ns
Cre-
Cre+
E
% TCR Vβ usage
Cre-
Cre+
Vβ2
Vβ3
Vβ4
Vβ5.1 and 5.2
Vβ6
Vβ7
Vβ8.1 and 8.2
Vβ8.3
Vβ9
Vβ10b
Vβ11
Vβ12
Vβ13
Vβ14
Vβ17a
F
% TCR Vβ usage
Cre-
Cre+
G
Q1
9.30
Q2
85.9
Q4
2.53
Q3
2.30
Cre-
Q1
6.94
Q2
89.3
Q4
2.08
Q3
1.64
Cre+
CD4
CD8α
% CD8 T cells of thymocytes
ns
Cre-
Cre+
% CD4 T cells of of thymocytes
ns
Cre-
Cre+
H
Q1
9.23
Q2
83.2
Q4
5.58
Q3
1.99
Cre-
Q1
7.71
Q2
82.9
Q4
7.42
Q3
2.00
Cre+
CD4
CD8α
% CD8 T cells of thymocytes
ns
Cre-
Cre+
% CD4 T cells of thymocytes
ns
Cre-
Cre+

261

Figure 1. Development of TMEM119+ microglia MHC class I molecule conditional knockout mice. Graphs in gray and pink represent Tmem119 K^b cKO mice and Cre- littermate controls. Graphs in orange and red represent Tmem119 D^b cKO mice and Cre- littermate controls. (A) Representative histograms and percentages of K^b expression of TMEM119+ cells in the brain in Tmem119 K^b cKO mice compared to Cre- littermate controls 7 days post TMEV infection, followed by (B) H-2K^b expression in several immune cell populations in the blood. (C) Representative histograms and percentages of D^b expression of TMEM119+ cells in the brain in Tmem119 D^b cKO mice compared to Cre- littermate controls 7 days post TMEV infection, followed by (D) H-2D^b expression in several immune cell populations in the blood. (E, F) Splenic TCR repertoire is not affected by cell-specific H-2K^b and H-2D^b deletion. Splenocytes were isolated from naïve 10-week-old animals (N = 3-7 per group) and stained with anti-CD45, anti-TCRβ, anti-CD4, and anti-CD8 antibodies, as well as antibodies specific to each of the T-cell receptor Vβ regions listed. (G, H) Representative plots and quantification show no disruption of thymocyte development in Tmem119 K^b cKO mice and Tmem119 D^b cKO in comparison to Cre negative littermates. Designation of symbols is as follows: ns or not shown for $p > 0.05$, * for $p \leq 0.05$, ** for $p \leq 0.01$, *** for $p \leq 0.001$, **** for $p \leq 0.0001$. Data presented as mean +/- SD.

280 **Conditional deletion of H-2K^b on microglia reduces antigen specific CD8 T cell**
281 **expansion in the brain 7 days post TMEV-OVA infection**

282 After validating our conditional knockout approach, we proceeded to investigate the
283 extent microglia H-2K^b was impacting CD8 T cell responses in the brain. Using our
284 targeted Cre-Lox approach that enables conditional deletion of H-2K^b in TMEM119+ cells
285 (Figure 2A), we infected mice with recombinant TMEV-OVA virus which encodes the
286 model antigen SIINFEKL presented in the context of the K^b class I molecule [23]. We
287 evaluated the impact on the ensuing brain infiltrating immune response at 7 days post
288 infection (Figure 2B). We observed a marked reduction in the frequencies of several
289 immune populations such as NK cells, dendritic cells, macrophages and inflammatory
290 monocytes (Figure 2C and Figure S1). Of major note, K^b:OVA epitope specific CD8 T
291 cells were markedly reduced in Tmem119 K^b cKO mouse brains post infection, indicating
292 that microglia K^b restricted antigen presentation was required for complete CD8 T cell
293 expansion (Figure 2D).

294

295 **CD8 T cell proliferation is attenuated when K^b is conditionally ablated in microglia**
296 **during acute infection**

297 To define the mechanism by which H-2K^b expressed in microglia enhances CD8 T cell
298 responses in the brain, we evaluated the extent cell proliferation was a factor. We pulsed
299 mice with intraperitoneal administered BrdU to evaluate cell proliferation. BrdU is
300 incorporated into newly synthesized DNA by cells entering and progressing through the
301 S (DNA synthesis) phase of the cell cycle, a process detectable by anti-BrdU antibodies

302 using spectral flow cytometry. Substantial CD8 T cell infiltration of the brain occurs at 7
303 days post TMEV (and TMEV-OVA) infection. However, virus antigen-specific CD8 T cells
304 first infiltrate the brain at day 4 post infection [29]. We therefore designed our experiment to
305 enable this first wave of CD8 T cells at day 4 to enter the brain (Figure 2E). We next
306 treated mice with FTY720 to sequester T cells within the secondary lymphoid organs and
307 prevent further brain infiltration of antiviral CD8 T cells. FTY720 treatment therefore
308 allowed us to analyze T cell proliferation specifically in the brain. Following this
309 experimental design, we confirmed that FTY720 treatment resulted in decreased T cell
310 numbers in the blood (Figure S2). Importantly, we determined that the percentage of
311 BrdU+ T cells and antiviral K^b:OVA antigen specific CD8 T cells were significantly
312 decreased in the brains of Tmem119 K^b cKO mice (Figure 2F). This confirmed microglia
313 K^b class I restricted antigen presentation was required for optimal CD8 T cell proliferation
314 in the brain.

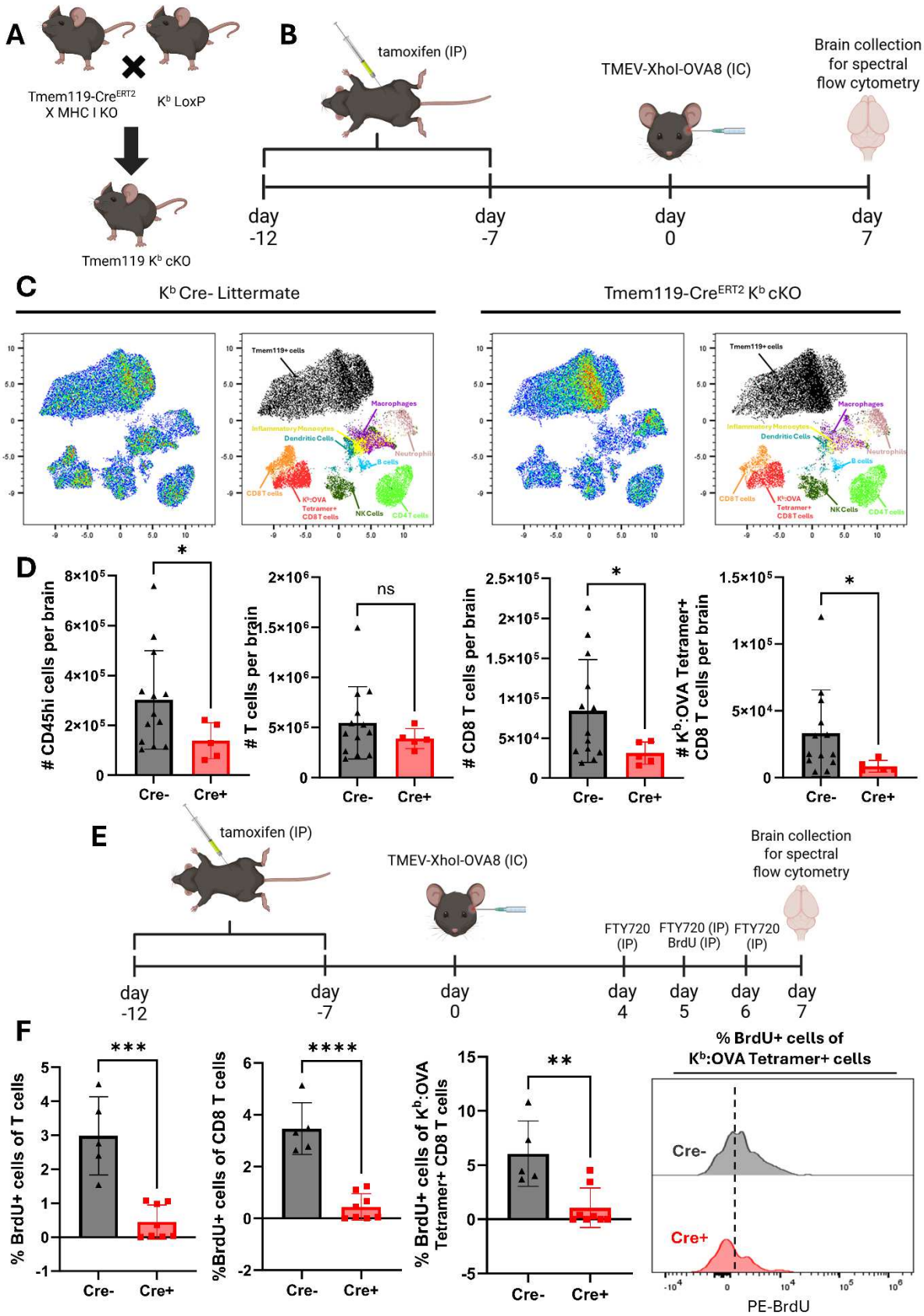
A
Tmem119-CreERT2 X MHC I KO
Kb LoxP
Tmem119 Kb cKO
B
tamoxifen (IP)
TMEV-XhoI-OVA8 (IC)
Brain collection for spectral flow cytometry
day -12
day -7
day 0
day 7
C
Kb Cre- Littermate
Tmem119-CreERT2 Kb cKO
Tmem119+ cells
Macrophages
Inflammatory Monocytes
Dendritic Cells
Neutrophils
B cells
CD8 T cells
Kb:OVA Tetramer+ CD8 T cells
NK Cells
CD4 T cells
D
CD45hi cells per brain
T cells per brain
CD8 T cells per brain
Kb:OVA Tetramer+ CD8 T cells per brain
Cre-
Cre+
ns
E
tamoxifen (IP)
TMEV-XhoI-OVA8 (IC)
Brain collection for spectral flow cytometry
FTY720 (IP)
FTY720 (IP) BrdU (IP)
FTY720 (IP)
day -12
day -7
day 0
day 4
day 5
day 6
day 7
F
% BrdU+ cells of T cells
%BrdU+ cells of CD8 T cells
% BrdU+ cells of Kb:OVA Tetramer+ CD8 T cells
% BrdU+ cells of Kb:OVA Tetramer+ cells
Cre-
Cre+
PE-BrdU

Figure 2. Tmem119 K^b cKO mice exhibit decreased K^b:OVA epitope specific CD8 T cell numbers and decreased BrdU labeling at brain 7 days post TMEV-OVA infection. (A) Schematic depicting the Cre-LoxP strategy. Tmem119-Cre^{ERT2} mice were crossed to transgenic H-2K^b LoxP mice. (B) Experimental design showing mice were treated with tamoxifen to activate cre for 5 days, once a day. Mice were infected with TMEV-OVA and euthanized 7 days post infection. Brains were analyzed using spectral flow cytometry. (C) Representative uniform manifold approximation and projection (UMAP) key, colored to highlight the different cell subsets in the brain for both K^b Cre-Littermate and Tmem119-CreERT2 K^b cKO mice. (D) Absolute counts of CD45hi, T cells, CD8 T cells and K^b:OVA Tetramer+ CD8 T cells per brain. (E) Experimental design showing mice were treated with FTY720 or water twice a day starting 4 days after TMEV-OVA infection. 5 days after TMEV-OVA infection, mice received an IP injection of BrdU. Mice were euthanized 7 days after TMEV-OVA infection and perfused. Brains were analyzed using a Cytek Aurora. (F) Bar charts show reduced % BrdU in T cells, CD8 T cells and K^b:OVA Tetramer+ cells in Tmem119 K^b cKO mice compared to cre- littermate controls, as well as representative histograms for Brdu expression in K^b:OVA Tetramer+ cells. Designation of symbols is as follows: ns or not shown for $p > 0.05$, * for $p \leq 0.05$, ** for $p \leq 0.01$, *** for $p \leq 0.001$, **** for $p \leq 0.0001$. Data presented as mean +/- SD.

334 **CD8 T cell proliferation induced by microglia H-2K^b restricted antigen presentation**
335 **occurs within the brain**

336 After establishing that H-2K^b expression by microglia is required for complete CD8 T cell
337 responses in the brain following neurotropic viral infection, we sought to define the
338 anatomical location of this stimulation. Parabiosis is a powerful method in which two mice
339 are surgically conjoined to share circulation. This approach enables a Tmem119 K^b cKO
340 mouse to have a surrogate immune system provided by a Cre- littermate parabiont. We
341 surgically conjoined Tmem119 K^b cKO mice to Cre- littermates and waited 3 weeks to
342 ensure shared circulation. At this timepoint, we infected both mice intracranially with
343 TMEV-OVA (Figure 3A). 7 days post TMEV-OVA infection, we PBS perfused both
344 parabionts and analyzed their brain infiltrating immune responses. Following paired wise
345 analysis, we determined that Tmem119 K^b cKO mice still exhibited decreased numbers
346 of infiltrating cells and CD8 T cells (Figure 3B) despite sharing peripheral immune system
347 with a Cre- littermate. A trending decline in the numbers of K^b:OVA Tetramer+ CD8 T
348 cells was also observed. These results demonstrate stimulation of CD8 T cells by H-2K^b
349 on microglia occurs within the brain and is not governed by peripheral factors.

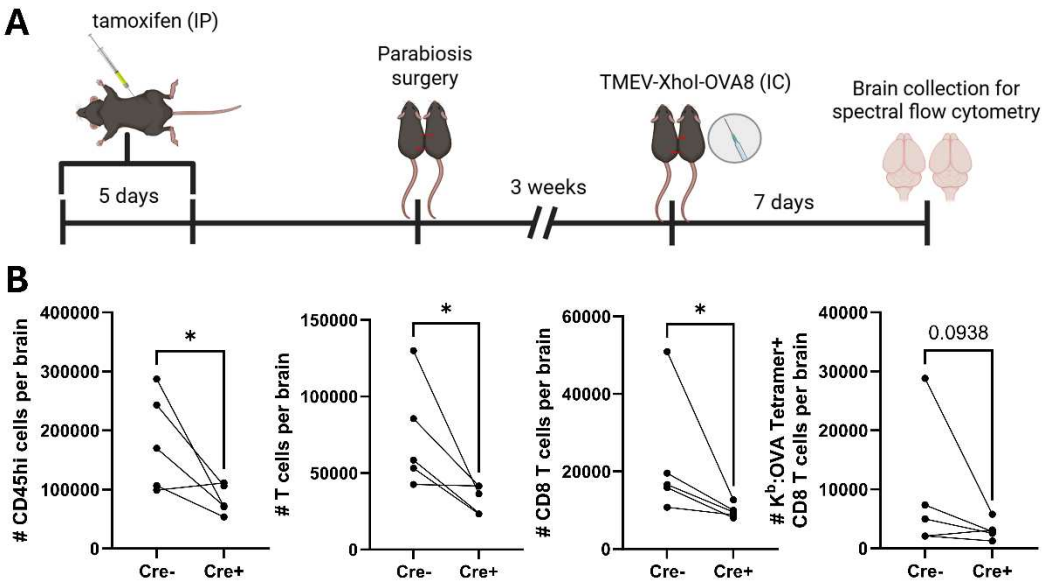

Figure 3. CD8 T cell expansion in the brain is governed by microglia K^b restricted antigen presentation and not through peripheral circulating factors. (A) Experimental design showing mice were treated with tamoxifen to activate cre for 5 days, once a day. A Tmem119 K^b cKO mouse was then attached to a Cre- littermate through parabiosis surgery. 3 weeks later, mice were infected with TMEV-OVA and euthanized 7 days post infection. Brains were analyzed using spectral flow cytometry. (B) Absolute counts of CD45hi, T cells, CD8 T cells and K^b:OVA Tetramer+ CD8 T cells per brain. Designation of symbols is as follows: ns or not shown for $p > 0.05$, * for $p \leq 0.05$, ** for $p \leq 0.01$, *** for $p \leq 0.001$, **** for $p \leq 0.0001$. Data presented as mean +/- SD.

360 **Microglia expression of H-2D^b class I molecule enhances CD8 T cell activation and**
361 **effector status in the brain**

362 During TMEV infection, H-2D^b class I molecule presents the immunodominant TMEV
363 peptide, VP2$_{121-130}$, to CD8 T cells, which is required for viral clearance [17, 18, 30]. We
364 generated a novel Tmem119 D^b cKO mice in which H-2D^b is deleted from TMEM119+
365 microglia (Figure 4A). Tmem119 D^b cKO mice were infected with TMEV. At 7 days post
366 infection, mice were perfused with 1X PBS and brains were harvested for flow cytometric
367 analysis of CD8 T cell infiltration (Figure 4B). We did not observe changes in frequencies
368 of major immune cell populations, including D^b:VP2$_{121-130}$ Tetramer+ CD8 T cells (Figure
369 4C and 4D). However, we observed reduced effector properties in CD8 T cells. This was
370 demonstrated by a marked decrease in perforin protein levels and reduced percentages
371 of perforin+ CD8 T cells and D^b:VP2$_{121-130}$ Tetramer+ CD8 T cells in 7-day TMEV infected
372 Tmem119 D^b cKO mice (Figure 4E). Perforin is a cytolytic protein expressed during the
373 effector stages of antiviral immune responses, orchestrating killing mechanisms essential
374 for complete cytotoxic CD8 T cell function [24]. This result indicates that H-2D^b antigen
375 presentation on microglia are responsible for enhancing CD8 T cell effector status in the
376 brain.

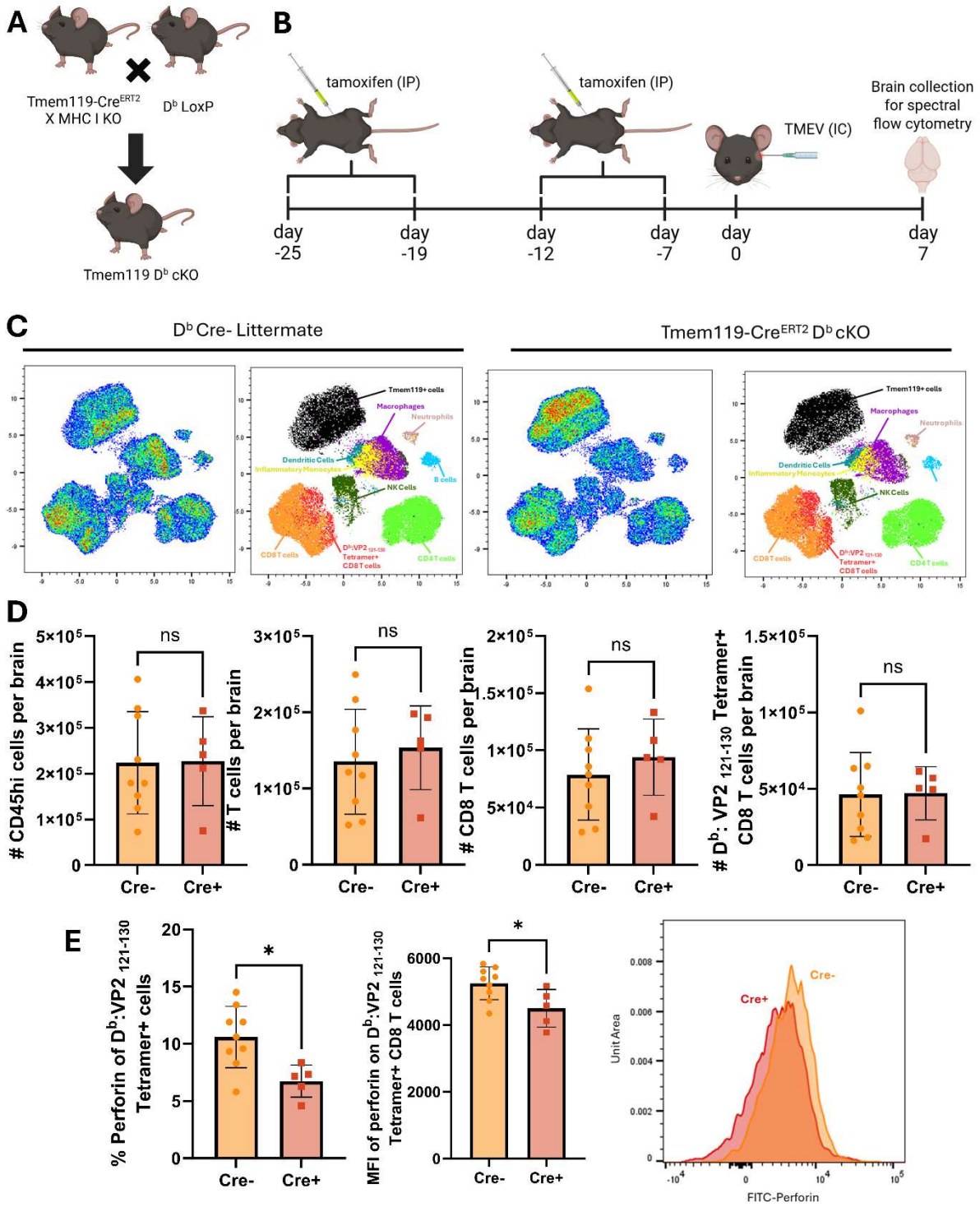

Figure 4. Tmem119 D^b cKO mice have decreased perforin expression by CD8 T cells 7 days post TMEV infection. (A) Schematic depicting the Cre-LoxP strategy. Tmem119-Cre^{ERT2} mice were crossed to transgenic H-2D^b LoxP mice. (B) Experimental design showing mice were treated with tamoxifen to activate cre for 5 days, once a day. After 1 week, another 5 days of tamoxifen injections were employed. Mice were then infected

with TMEV and euthanized 7 days post infection. Brains were analyzed using a Cytek Aurora. (C) Representative uniform manifold approximation and projection (UMAP) key, colored to highlight the different cell subsets in the brain for both D^b Cre- Littermate and Tmem119-CreER^{T2} D^b cKO mice. (D) Absolute counts of CD45hi, T cells, CD8 T cells and D^b:VP2$_{121-130}$ Tetramer+ CD8 T cells per brain are displayed in the bar charts, as well as frequency of perforin on CD8 T cells and D^b:VP2$_{121-130}$ Tetramer+ cells. (E) Percentages of Perforin+ cells of D^b:VP2$_{121-130}$ Tetramer+ CD8 T cells are displayed in the bar charts, followed by graph displaying MFI of perforin on of D^b:VP2$_{121-130}$ Tetramer+ CD8 T cells and a histogram of a representative sample for Perforin expression on D^b:VP2$_{121-130}$ Tetramer+ CD8 T cells (scaled to Unit Area to normalize by area and not number of events). Designation of symbols is as follows: ns or not shown for $p > 0.05$, * for $p \leq 0.05$, ** for $p \leq 0.01$, *** for $p \leq 0.001$, **** for $p \leq 0.0001$. Data presented as mean +/- SD.

396 **Microglia expression of D^b enhances CD8 T cell mediated blood-brain barrier**
397 **disruption in a CNS vascular disease model**

398 Our finding that perforin was reduced in CD8 T cells isolated form TMEV infected
399 Tmem119 D^b cKO mice was intriguing and prompted us to evaluate these animals for
400 CNS vascular permeability. Our laboratory has determined that perforin expressing CD8
401 T cells mediate BBB disruption in experimental cerebral malaria and peptide induced fatal
402 syndrome (PIFS) [24, 25, 31]. PIFS is a model generated in our laboratory that consists of
403 intravenously injecting the viral immunodominant peptide $VP2_{121-130}$ in mice at day 7 post
404 TMEV infection (Figure 5A) [32]. $VP2_{121-130}$ peptide administration stimulates activated
405 D^b:$VP2_{121-130}$ epitope specific CD8 T cells which in turn induce severe blood-brain barrier
406 (BBB) disruption within 4 hours and is ultimately fatal at 24 hours [33]. This BBB disruption
407 is defined by the loss of cerebrovascular endothelial cell tight junction integrity.
408 and is governed by perforin expressing CD8 T cell response, consistent with our findings
409 in experimental cerebral malaria [24, 31 33]. Therefore, we investigated the impact of
410 differential expression of perforin by D^b:$VP2_{121-130}$ Tetramer+ CD8 T cells on BBB
411 disruption in Tmem119 D^b cKO mice using the PIFS model. We noticed a marked
412 reduction in overall numbers of infiltrating blood-derived cells (CD45hi cells), total T cells,
413 CD8 T cells and D^b:$VP2_{121-130}$ Tetramer+ CD8 T cells, indicating that the loss of H-$2D^b$ on
414 microglia attenuates the immune response in the brain (Figure 5B). To assess BBB
415 integrity, in a separate experiment, we intravenously injected FITC-albumin in both
416 Tmem119 D^b cKO mice and Cre- littermate controls 1 hour before euthanasia (Figure
417 5C). We observed reduced CNS vascular permeability as demonstrated by FITC-albumin
418 leakage into brain parenchyma in sagittal cut sections of Tmem119 D^b cKO mouse brains

419 when compared to Cre- littermates (Figure 5D). Compromised BBB integrity in Cre-
420 controls was therefore consistent with heightened levels of perforin expression by
421 D^b:$VP2_{121-130}$ Tetramer+ CD8 T cells (Figure 4E and 5D). In contrast, Tmem119 D^b cKO
422 mice have preserved vascular integrity due to the absence of H-$2D^b$ restricted antigen
423 presentation by microglia in the PIFS model which is also consistent with CD8 T cells
424 having markedly reduced perforin expression (Figure 4E and 5D).

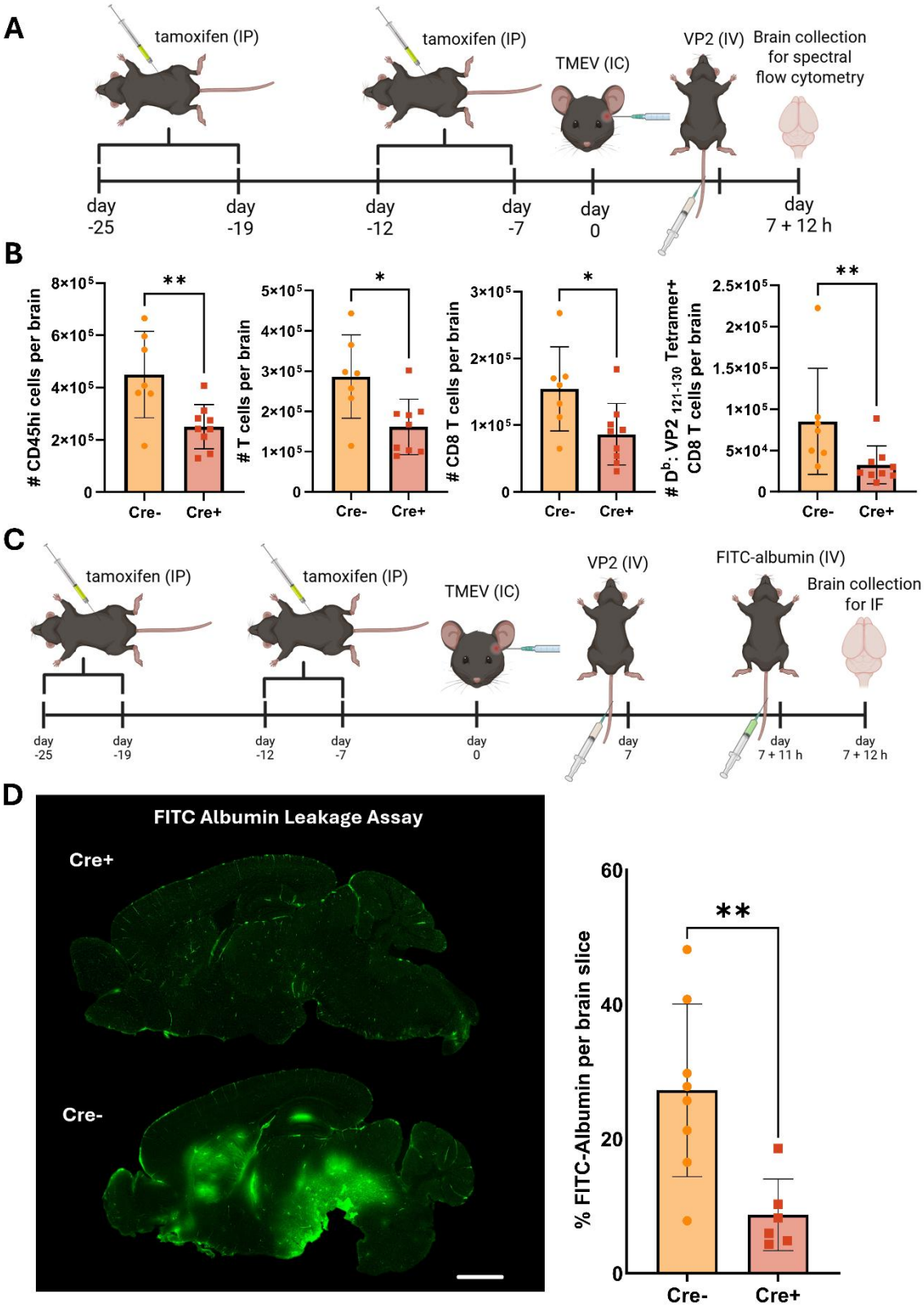
A
tamoxifen (IP)
tamoxifen (IP)
TMEV (IC)
VP2 (IV)
Brain collection for spectral flow cytometry
day -25
day -19
day -12
day -7
day 0
day 7 + 12 h
B
CD45hi cells per brain
T cells per brain
CD8 T cells per brain
Db: VP2 121-130 Tetramer+ CD8 T cells per brain
Cre-
Cre+
C
tamoxifen (IP)
tamoxifen (IP)
TMEV (IC)
VP2 (IV)
FITC-albumin (IV)
Brain collection for IF
day -25
day -19
day -12
day -7
day 0
day 7
day 7 + 11 h
day 7 + 12 h
D
FITC Albumin Leakage Assay
Cre+
Cre-
% FITC-Albumin per brain slice
Cre-
Cre+

425

426 **Figure 5. Peptide-induced fatal syndrome elicits increased cell infiltration in**
427 **comparison to Tmem119 D^b cKO mice.** (A) Mice were intracranially infected with
428 TMEV. 7 days later, mice received the TMEV immunodominant peptide $VP2_{121–130}$
429 intravenously. Injection of VP2121–130 peptide will induce lethal blood-brain barrier. 12
430 hours post injection of $VP2_{121–130}$, mice were euthanized, perfused, and analyzed. (B)
431 Absolute counts of CD45hi, T cells, CD8 T cells and D^b:$VP2_{121-130}$ Tetramer+ CD8 T cells
432 per brain are displayed in the bar charts. (C) Mice were intracranially infected with TMEV.
433 7 days later, mice received the TMEV immunodominant peptide $VP2_{121–130}$ intravenously.
434 11 hours after the $VP2_{121–130}$ injection, FITC-albumin was administered intravenously. 12
435 hours post injection of $VP2_{121–130}$, mice were euthanized and analyzed. (D)
436 Representative sagittal images of FITC-albumin injected mice 12 hours post $VP2_{121–130}$
437 injection, displaying BBB leakage differences between Cre+ and Cre- groups.
438 Quantification is displayed on the left. Scale bar = 2 mm. Designation of symbols is as
439 follows: ns or not shown for $p > 0.05$, * for $p \leq 0.05$, ** for $p \leq 0.01$, *** for $p \leq 0.001$, ****
440 for $p \leq 0.0001$. Data presented as mean +/- SD.

441 **CD8 T cell-mediated BBB disruption is exacerbated by microglia D^b restricted**
442 **antigen presentation and is not impacted by peripheral circulating factors**

443 To determine the location of CD8 T cell stimulation by MHC class I expressing microglia,
444 we performed parabiosis surgery to conjoin Tmem119 D^b cKO mice to Cre- littermate
445 controls. 3 weeks post-surgery, we intracranially infected both mice with TMEV. At 7 days
446 post infection, we i.v. administered $VP2_{121-130}$ peptide intravenously in both mice to induce
447 PIFS. 11 hours post-$VP2_{121-130}$ peptide delivery and 1 hour prior to euthanasia, all mice
448 were i.v. injected with FITC-albumin to measure BBB disruption (Figure 6A). Despite
449 sharing circulation to a Cre- littermate control, Tmem119 D^b cKO mice presented with
450 greatly reduced BBB disruption (Figure 6B). Paired wise quantification of sagittal cuts
451 obtained from 4 sets of parabionts were analyzed (Figure 6C). This data demonstrates
452 that shared circulation and peripheral factors do not restore CD8 T cell mediated BBB
453 disruption when microglia was no longer able to present antigen via H-$2D^b$.

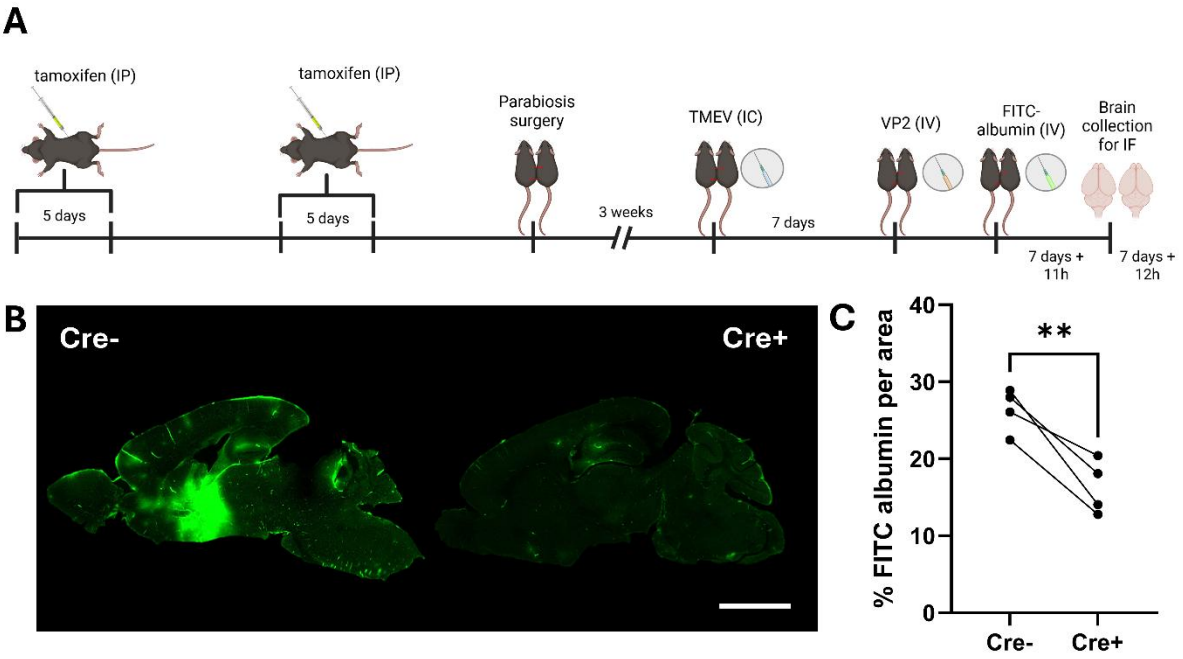

Figure 6. Tmem119 D^b cKO mice are protected from BBB disruption despite sharing circulation with a Cre- littermate parabiont. (A) Experimental design showing mice were treated with tamoxifen to activate cre for 5 days, once a day, and then another 5 days 1 week later. A Tmem119 D^b cKO mouse was then attached to a Cre- littermate through parabiosis surgery. 3 weeks later, mice were infected with TMEV. 7 days later, mice received the TMEV immunodominant peptide $VP2_{121–130}$ intravenously. 11 hours after the $VP2_{121–130}$ injection, FITC-albumin was administered intravenously. 12 hours post injection of $VP2_{121–130}$, mice were euthanized and analyzed. (B) Representative sagittal images of FITC-albumin injected mice 12 hours post $VP2_{121–130}$ injection, displaying BBB leakage differences between Cre+ and Cre- groups. Quantification is displayed on the left. Scale bar = 2 mm. Designation of symbols is as follows: ns or not shown for $p > 0.05$, * for $p \leq 0.05$, ** for $p \leq 0.01$, *** for $p \leq 0.001$, **** for $p \leq 0.0001$. Data presented as mean +/- SD.

468 **Microglia MHC class I antigen presentation does not affect the generation of**
469 **memory CD8 T cells**

470 TMEV infection is cleared from the brain approximately between 14 - 21 days post
471 infection [8, 19]. It has been recently shown that TMEV infection results in the accumulation
472 and retention of antigen specific CD8 TRM cells within the brain at 30 days post infection
473 [3]. However, it is not known if microglial MHC class I responses are involved in the
474 generation of CD8 TRM cells in the brain. To define the contribution of H-2D^b on microglia
475 for CD8 T cell memory formation in the brain, we infected both Tmem119 D^b cKO mice
476 and Cre- littermate controls and analyzed the numbers of CD8 TRM cells 30 days post
477 infection (Figure 7A). We did not observe differences between the groups at this time
478 point, as the number of D^b:VP2$_{121-130}$ Tetramer+ CD8 T cells was similar in Tmem119 D^b
479 cKO and Cre- mice (Figure 7B). CD69+ CD103+ of D^b:VP2$_{121-130}$ Tetramer+ cells were
480 also not altered (data not shown).

481 Our laboratory has also developed a model to study the reactivation of CD8 TRM cells
482 through administration of immunodominant viral peptide, VP2$_{121-130}$, post viral clearance
483 [3]. This stimulation results in the reactivation of D^b:VP2$_{121-130}$ epitope specific CD8 TRM
484 cells and sublethal BBB disruption. To assess the contribution of H-2D^b antigen
485 presentation on microglia for reactivation of antigen specific CD8 TRM cells, immune cell
486 infiltration in general, and BBB disruption, we infected mice with TMEV and then injected
487 tamoxifen to activate cre recombinase (Figure 7C). This allows us to investigate the
488 effects of H-2D^b expression on microglia at the time of the reactivation. Anti-CD45
489 antibody i.v. labeling was used to identify cells residing in vasculature verses brain
490 parenchyma. Animals were perfused to ensure that immune cells in vasculature were

491 excluded from analysis. 48 hours after $VP2_{121-130}$ or control E7 peptide, we observed an
492 increase in the numbers of infiltrating cells in both Tmem119 D^b cKO mice and Cre-
493 littermate controls (Figure 7D). However, Tmem119 D^b cKO mice that received $VP2_{121-}$
494 $_{130}$ injection exhibited a decrease in the immune cell infiltration in comparison to Cre-
495 littermates that also received $VP2_{121-130}$ (Figure 7D). Interestingly, in agreement with
496 previous data from our laboratory, we observed an expansion of CD11b+ MHC II+ cells
497 following $VP2_{121-130}$ injection [3]. This population was attenuated in the Tmem119 D^b cKO
498 mice, suggesting that microglia MHC class I is involved in the recruitment of overall
499 infiltrating cells and the expansion of a myeloid cell population, potentially following
500 engagement by CD8 T cell. Although we did find altered immune cell infiltration overall,
501 we did not observe differences in the numbers of D^b:$VP2_{121-130}$ Tetramer+ CD8 T cells
502 between Tmem119 D^b cKO and Cre- littermate controls in the numbers of (Figure 7E).

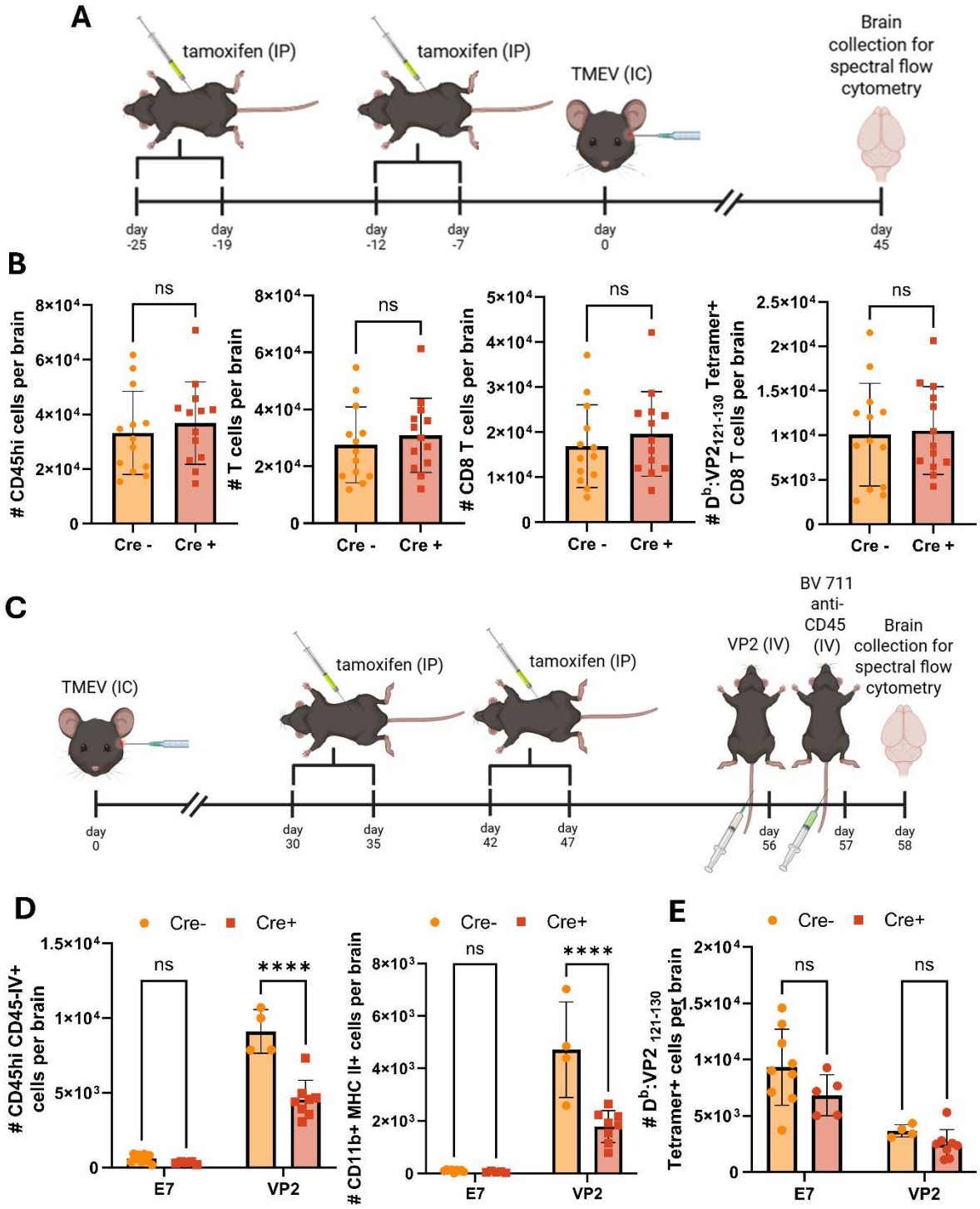

Figure 7. Microglia D^b restricted antigen presentation is not required for CD8 TRM cell formation in comparison to Cre- littermates. However, upon secondary challenge, Tmem119 D^b cKO mice have attenuated immune cell infiltration. (A) Experimental design showing mice were treated with tamoxifen to activate cre

recombinase for 5 days, once a day, and then another 5 days 1 week later. Mice were intracranially infected with TMEV and allowed 45 days for resolution of the infection and TRM generation. Mice were then euthanized, perfused, and analyzed. (B) Absolute counts of CD45hi, T cells, CD8 T cells and D^b:$VP2_{121-130}$ Tetramer+ CD8 T cells per brain are displayed in the bar charts. (C) Mice were intracranially infected with TMEV and allowed 30 days for resolution of the infection and TRM generation. Later, mice were treated with tamoxifen to activate cre recombinase for 5 days, once a day, and then another 5 days 1 week later. Following tamoxifen injections, mice received either the TMEV immunodominant peptide $VP2_{121–130}$, or irrelevant peptide E7 two days before euthanasia. Injection of $VP2_{121–130}$ peptide will reactivate TMEV specific T cells including TRMs in the brain. 24 hours post $VP2_{121–130}$ injections mice received an intravenous injection of BV711 anti-CD45 conjugated antibody to label CD45+ cells within the blood circulation. 24 hours post injection of antibodies, mice were euthanized, perfused, and analyzed. (D) Absolute counts of infiltrating cells (CD45hi CD45-IV+ cells per brain) and myeloid cells (CD11b+ MHC II+ cells per brain). (E) Absolute counts of D^b: $VP2_{121-130}$ Tetramer+ CD8 T cells per brain. Designation of symbols is as follows: ns or not shown for $p > 0.05$, * for $p \leq 0.05$, ** for $p \leq 0.01$, *** for $p \leq 0.001$, **** for $p \leq 0.0001$. Data presented as mean +/- SD.

526 **Microglial MHC class I contributes to the expansion of CD8 TRM cell populations**
527 **in the brain during antigen recall response**

528 To assess the contribution of microglia MHC class I in the recall response of CD8 TRM
529 cells, we TMEV infected Tmem119 D^b cKO mice and Cre- littermate controls before
530 tamoxifen injections. D^b expressing mice resolve TMEV infection in 14-21 days [8, 19]. We
531 then waited until day 30 to administer tamoxifen to inactivate D^b class I molecule in
532 microglia (Figure 8A). FTY720 was administered 3 days prior $VP2_{121-120}$ i.v injection and
533 2 days after to restimulate memory D^b:$VP2_{121-130}$ epitope specific CD8 TRM cells (Figure
534 8A). This approach allows blockade of peripheral lymphocyte trafficking into the brain
535 including peripheral memory CD8 T cells, thereby isolating D^b:$VP2_{121-130}$ epitope specific
536 CD8 TRM cell responses. First, we confirmed that FTY720 treatment resulted in
537 decreased T cell frequencies in the blood (Figure S3). Meanwhile, through analysis of the
538 brain we identified that Tmem119 D^b cKO mice had a marked decrease in both
539 frequencies and numbers of D^b:$VP2_{121-130}$ Tetramer+ CD8 T cells, accompanied by a
540 decrease in both frequencies and numbers of total infiltrating cells (CD45hi+ cells) and
541 myeloid cells (CD11b+ MHC II+ cells) (Figure 8B, C and D). Importantly, we observed
542 reduced BBB permeability through reduced gadolinium leakage into the tissue in
543 Tmem119 D^b cKO mice (Figure 8E). It is important to note that both Tmem119 D^b cKO
544 mice and Cre- littermate controls received FTY720 and $VP2_{121-120}$ injections. Therefore,
545 reduced D^b:$VP2_{121-130}$ Tetramer+ cell expansion in the brain and reduced BBB
546 permeability is the result of microglia H-$2D^b$ antigen presentation being conditionally
547 ablated. This demonstrates a critical requirement of microglia D^b restricted antigen

548 presentation in the recall CD8 TRM response to the immunodominant D^b:$VP2_{121-130}$

549 epitope during neurotropic virus infection.

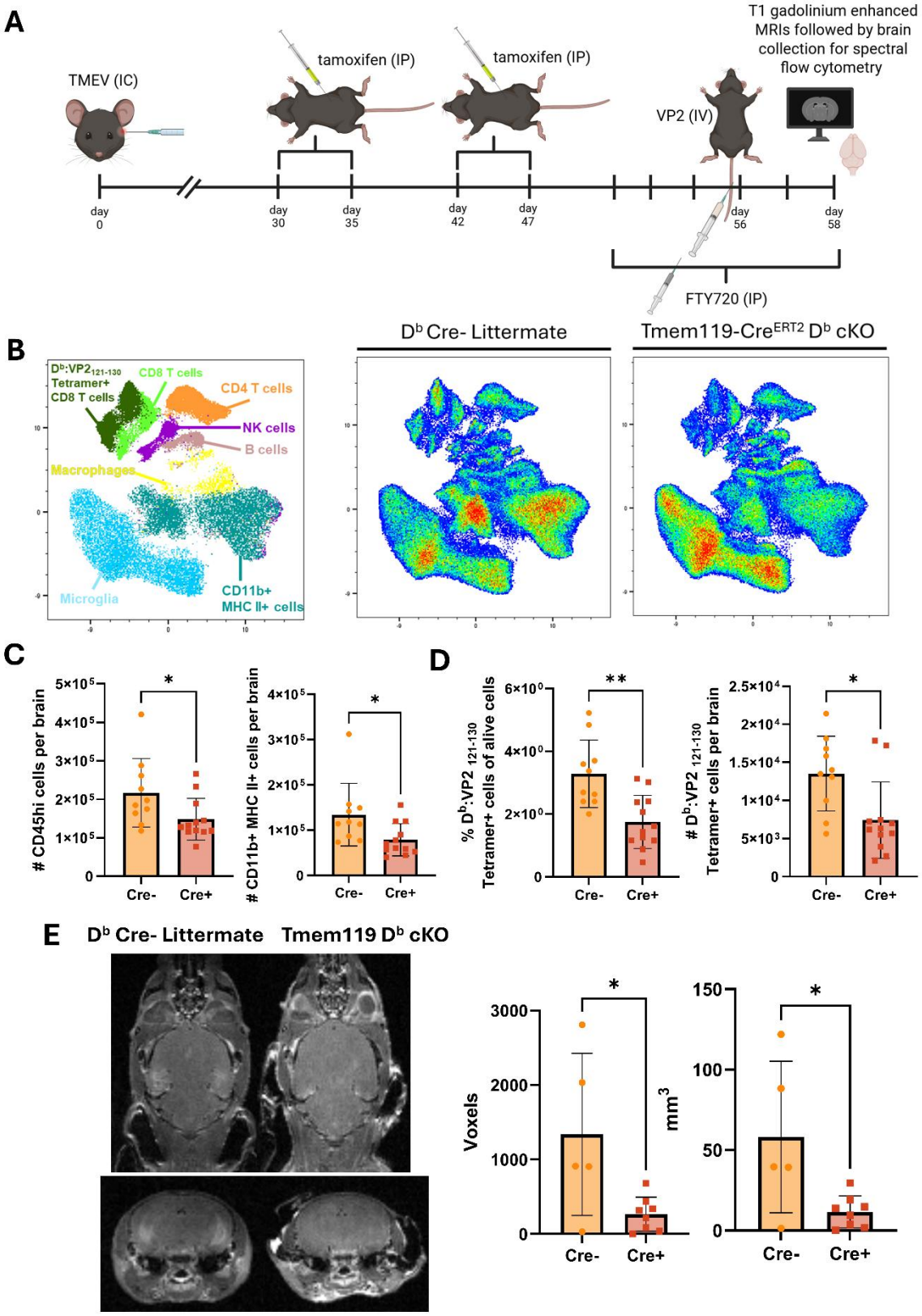
A
TMEV (IC)
tamoxifen (IP)
tamoxifen (IP)
VP2 (IV)
T1 gadolinium enhanced MRIs followed by brain collection for spectral flow cytometry
day 0
day 30
day 35
day 42
day 47
day 56
day 58
FTY720 (IP)
B
Dᵇ:VP2121-130 Tetramer+ CD8 T cells
CD8 T cells
CD4 T cells
NK cells
B cells
Macrophages
Microglia
CD11b+ MHC II+ cells
Dᵇ Cre- Littermate
Tmem119-CreERT2 Dᵇ cKO
C
CD45hi cells per brain
CD11b+ MHC II+ cells per brain
Cre-
Cre+
D
% Dᵇ:VP2 121-130 Tetramer+ cells of alive cells
# Dᵇ:VP2 121-130 Tetramer+ cells per brain
E
Dᵇ Cre- Littermate
Tmem119 Dᵇ cKO
Voxels
mm3

551 **Figure 8. CD8 TRM cell responses are decreased in Tmem119 D^b cKO mice and**
552 **accompanied by reduced numbers of infiltrating cells and BBB permeability.** (A)
553 Experimental design showing mice were intracranially infected with TMEV and allowed
554 30 days for resolution of the infection and TRM generation. Later, mice were treated with
555 tamoxifen to activate cre recombinase for 5 days, once a day, and then another 5 days 1
556 week later. Following tamoxifen injections, mice received an intravenous injection of the
557 TMEV immunodominant peptide $VP2_{121–130}$ to reactivate TMEV specific T cells including
558 CD8 TRMs in the brain. 3 days before and 1 day after $VP2_{121–130}$ injections, mice received
559 intraperitoneal injections of FTY720 twice a day. 48 hours post $VP2_{121–130}$ injections, mice
560 were imaged using T1 gadolinium enganced MRIs and then euthanized, perfused, and
561 analyzed. (B) UMAPs displaying frequencies of alive of several immune cell populations
562 are displayed. (C) Absolute counts of infiltrating cells (#CD45hi+ cells) and myeloid cells
563 (#CD11b+ MHC II+ cells) per brain, as well as (D) counts and numbers of D^b:$VP2_{121-130}$
564 Tetramer+ cells are displayed. (E) BBB permeability was measured by gadolinium
565 enhanced MRIs analysis using T1 weighted MRIs. Representative images are displayed
566 on the left followed by quantification on the right. Designation of symbols is as follows: ns
567 or not shown for $p > 0.05$, * for $p \leq 0.05$, ** for $p \leq 0.01$, *** for $p \leq 0.001$, **** for $p \leq$
568 0.0001. Data presented as mean +/- SD.

569 **Discussion**

570 In this study, we capitalized on the magnitude of immunodominant CD8 T cell responses
571 generated against neurotropic TMEV infection to define the impact of discrete MHC class
572 I molecule restricted antigen presentation by microglia. Through our ability to conditionally
573 inactivate H-2K^b and H-2D^b, our study was able to define the contribution of individual
574 microglia MHC class I antigen presentation during acute and memory responses. We
575 defined that H-2K^b antigen presentation on microglia is essential for the expansion of
576 K^b:OVA Tetramer+ CD8 T cells during neurotropic virus infection. Our data specifies that
577 this expansion is due to proliferation of CD8 T cells and occurs as a consequence of
578 microglia H-2K^b restricted antigen presentation. Furthermore, we define that H-2D^b
579 antigen presentation on microglia is important for heightened activation of antiviral
580 D^b:VP2$_{121-130}$ epitope specific CD8 T cells as observed by enhanced perforin expression.
581 This modulation results in lower overall immune cell infiltration and reduced BBB
582 disruption in the PIFS model. Importantly, these effects are localized to the CNS. Finally,
583 post clearance of the TMEV virus infection, we demonstrate microglia H-2D^b is required
584 for complete immune cell infiltration during a secondary encounter with virus antigen. CD8
585 TRM cells are activated by H-2D^b restricted antigen presentation by microglia, resulting
586 in increased immune cell infiltration.

587 CD8 T cell expansion in the brain is a key element to many neurological diseases [34]. To
588 our knowledge, this work is the first demonstration of MHC class I antigen presentation
589 by microglia directly activating CD8 T cells to promote BBB disruption. Furthermore, we
590 dissected the contribution of discrete MHC class I molecules on microglia in shaping CD8
591 T cell response in the brain.

592 Historically, whole cell ablation strategies have been employed to define the contribution
593 of microglia to neuroinflammation, including the influence on adaptive immune cell
594 responses. Pexidartinib (PLX3397) is a CSF1 receptor inhibitor widely used for microglia
595 depletion. However, this depletion strategy is not limited to microglia or even CNS myeloid
596 cells in general [20]. Previous studies have shown that PLX3397 administration decreases
597 splenocyte numbers and depletes CD11c+ cells, implying peripheral T cell priming by
598 dendritic cells would be impaired [8]. Additional investigation of PLX3397 administration
599 revealed circulating and bone marrow derived immune cells beyond the mononuclear
600 phagocyte system were also affected, suggesting the need for caution when interpreting
601 results employing this depletion strategy [20]. Recently, an alternative approach using
602 PLX5622 has been proposed to be more microglia specific. However, PLX5622 also has
603 significant non-microglia off target effects that could contribute to results observed
604 employing this drug [21, 35]. Importantly, whole cell depletion of microglia nullifies the ability
605 to study discrete microglial functions in experimental neurologic disease models.

606 Aside from cellular depletion strategies, CX3CR1 Cre expressing mice are commonly
607 used to conduct gene ablation in microglia. Previous work employing this Cre strategy
608 has been important in highlighting microglia as an antigen presenting cell, capable of
609 modulating CD8 T cell responses in the brain [8]. During neurotropic viral infection, H-2D^b
610 antigen presentation by microglia was put forward as a major regulator for CD8 T cell
611 response and brain atrophy as a long-term consequence [8]. However, studies employing
612 CX3CR1 promoter induced green fluorescent protein (GFP) revealed monocytes, NK
613 cells, circulating and skin resident dendritic cells were also impacted in addition to
614 microglia [22, 26]. In tamoxifen-induced systems, waiting a 6-week interval after Cre

615 recombinase activation allows peripheral CX3CR1 expressing cells in the periphery to
616 turnover, reducing the off-target effects of this approach [8]. However, brain resident
617 CX3CR1 expressing cells such as long-lived CNS residing perivascular macrophages
618 remain impacted. Therefore, while the CX3CR1 Cre line has been commonly used as a
619 microglia-specific strategy, the expression of CX3CR1 by non-microglial cells in the brain
620 still needs to be addressed when interpreting results obtained with this strategy. The
621 Tmem119-Cre^{ERT2} system employed in this study is a more specific approach to assess
622 microglial function [27, 28]. Tmem119 is a transmembrane protein that is highly expressed
623 by microglia in both mice and humans. Importantly, the Tmem119-EGFP system was
624 found to target parenchymal microglia, but not other brain macrophages and blood
625 monocytes [27].

626 Microglia MHC class II antigen presentation has been investigated through analysis of
627 human tissue and experiments using preclinical models. MHC class II expressing
628 microglia have been reported in brains of patients with Parkinson's disease (PD) and
629 Alzheimer's disease (AD) [14]. It has been reported in a mouse model that the expression
630 of full-length human α-synuclein increases the expression of MHC II by microglia [36].
631 Deletion of MHC II significantly reduced microgliosis following AAV2-SYN induction in this
632 PD model [36]. However, in studies using experimental autoimmune encephalomyelitis
633 (EAE) and cuprizone-induced demyelination models, deletion of MHC II in CX3CR1+ cells
634 did not alter disease onset, progression, or severity [37]. Much less studied is the extent
635 MHC class I antigen presentation by microglia shapes immune responses and
636 neuropathology, especially regarding the use of precision tools that specifically target
637 microglia [38]. Defining the role of MHC class I responses in microglia is of critical need,

638 given microglia have been defined as a major cellular source of MHC class I expression
639 in the CNS of both mice and humans when compared to other brain resident cell types
640 [13]. In this study, we therefore employed Tmem119-Cre^{ERT2} mice crossed with H-2K^{b} or H-
641 2D$^{b\ fl/fl}$ mice. This approach allowed us to investigate the role of discrete MHC class I
642 molecules in TMEM119+ microglia, other than assessing MHC class I function as a
643 singular molecule.

644 Strategies to conditionally ablate β2-microglobulin expression have been employed to
645 understand MHC class I biology MHC class I function *in vivo*. However, this is a very
646 broad knockout strategy. β2-microglobulin stabilizes hundreds of protein complexes as
647 diverse as Hfe, FcRn, MICA and MICB, Qa-1, MR1, TL antigens, and CD1 [39, 40, 41, 42, 43,
648 44, 45]. These numerous protein species govern major branches of inflammation including
649 iron metabolism, antibody transport to the brain, innate immune recognition of stressed
650 and apoptotic cells, adaptive immune cell function, NK cell killing, and NK T cell activation.
651 Off target effects of removing these major drivers of neuroinflammation confounds
652 interpretation of results obtained using targeted ablation of β2m [40, 46]. Furthermore, the
653 highly polymorphic mouse H-2 and human HLA genes are far from redundant in function
654 [47]. In the TMEV infection model alone, H-2 genes govern virus persistence and
655 susceptibility to demyelination, with D^{b} being genetically defined as a critical protecting
656 allele [17]. Furthermore, in experimental cerebral malaria (ECM), K^{b}-restricted antigen
657 engagement on brain endothelium was shown to be pivotal for CD8 T cell vascular
658 adhesion, arrest, infiltration and activation. Meanwhile, only CD8 T cell receptor
659 recognition of D^{b}-restricted antigens resulted in killing of mouse brain microvascular
660 endothelial cell and subsequent neuronal cell death, supporting that K^{b} and D^{b} regulate

661 distinct patterns of disease onset [48]. Finally, notable HLA genes have been associated
662 historically with resistance to human pathogens [49, 50, 51]. Our data supports the
663 heterogeneity behind MHC class I molecules as Tmem119 K^b cKO mice exhibit a
664 decreased antigen specific CD8 T cell response following a neurotropic virus infection
665 and Tmem119 D^b cKO mice do not follow the same pattern. In contrast, Tmem119 D^b
666 cKO mice exhibit decreased CD8 T cell activation observed by reduced perforin
667 expression, while Tmem119 K^b cKO mice did not result in this same phenotype,
668 supporting the importance of conditional ablation of discrete MHC I genes in designated
669 cell types.

670 The reduction of K^b:OVA Tetramer+ CD8 T cells numbers observed in TMEV-OVA
671 infected Tmem119 K^b cKO mice used in this study is likely due to a stimulatory event
672 taking place in the brain parenchyma. The Daniel strain of TMEV is a neurotropic
673 picornavirus that does not directly infect microglia yet results in a robust brain infiltrating
674 CD8 T cell response [16]. Moreover, incorporating OVA antigen sequence into recombinant
675 TMEV provides an important tool to also study H-2K^b restricted CD8 T cell responses in
676 the brain [23]. It is important to note that although the insertion of OVA to the TMEV virus
677 facilitates the tracking of antigen specific response, it does not alter the course of infection
678 [23].

679 Our study further explains the importance of microglia class I molecules on CD8 T cell
680 proliferation and effector function in the brain. While it is known that CD11c+ APCs are
681 critical for early priming of CD8 T cells against the immunodominant TMEV peptide
682 $VP2_{121-130}$, it was not fully understood whether other NVU cell types could provide a
683 secondary stimulatory event that expands the antigen specific CD8 T cell response in the

684 brain parenchyma [19]. Our data supports a working model that after TMEV infection,
685 antigen-specific CD8 T cells are generated peripherally before infiltrating the brain to
686 engage H-2K^b on microglia. The experimental design employing injections of FTY720 at
687 day 4 post infection allowed the first few CD8 T cells to infiltrate and blocked further
688 infiltration from day 4 until day 7. That, combined with BrdU labeling showed that K^b
689 restricted antigen presentation on microglia leads to increased cell proliferation of early
690 infiltrating of K^b:OVA Tetramer+ CD8 T cells, partially explaining the decreased numbers
691 of K^b:OVA Tetramer+ CD8 T cells found at 7 days post infection in Tmem119 K^b cKO
692 mice. Although we observed that cell proliferation is decreased in CD8 T cells of
693 Tmem119 K^b cKO mice, it is possible that this stimulatory signal can also lead to
694 regulation of overall immune cell infiltration. This is supported by our observed decrease
695 in other immune cell populations including inflammatory monocytes and macrophages.
696 Previous work from our laboratory has suggested that brain resident CD8 T cells can
697 trigger an immune response that leads to enhanced myeloid cell infiltration and microglial
698 activation [3]. Finally, our employment of parabiosis techniques in this study confirms that
699 differential peripheral priming of CD8 T cells is not affecting the observed
700 neuroinflammatory phenotype in mice with MHC class I deletion in microglia.

701 Perforin expression was found to be decreased in Tmem119 D^b cKO mice. Although the
702 numbers of D^b:VP2$_{121-130}$ Tetramer+ CD8 T cells were not different in the Tmem119 D^b
703 cKO mice, we observed a marked reduction in the percentages of perforin+ D^b:VP2$_{121-130}$
704 Tetramer+ CD8 T cells as well as a reduction in protein expression visualized by MFI
705 values. Perforin is a key cytolytic protein produced by CD8 T cells. This pore-forming
706 protein is critical for cell death and viral clearance during infectious diseases, and it has

707 been defined as a key mechanism for BBB disruption in ECM and the PIFS model [24, 25].
708 In the Tmem119 D^b cKO, the interaction between infiltrating D^b:$VP2_{121-130}$ Tetramer+ CD8
709 T cells might be a key step in further activating these CD8 T cells and not increasing its
710 proliferation as seen in the Tmem119 K^b cKO mice. We therefore determined if
711 modulation of CD8 T cell perforin by microglia H-$2D^b$ would affect neurotropic viral
712 infection. The PIFS model provides means to assess modulatory effects of perforin on
713 BBB disruption including gene dosage [24]. Perforin-heterozygous mice have reduced BBB
714 disruption as compared to wild type C57BL/6 mice in the PIFS model [24]. Similarly, we
715 have found that Tmem119 D^b cKO mice with their reduced perforin expression by D^b:VP2
716 epitope specific CD8 T cells have attenuated immune cell infiltration and BBB disruption.
717 We contend that the stimulatory effect of CD8 T cells provided by H-$2D^b$ is further
718 activating D^b:$VP2_{121-130}$ epitope specific CD8 T cells, increasing their perforin production
719 and capacity to induce BBB disruption.

720 Microglia have been linked to BBB disruption in numerous contexts [52, 53]. Although
721 microglia are not anatomically described as being tightly opposed with endothelial cells
722 at the NVU, there are reports of ramified populations residing in close proximity to brain
723 capillaries [54]. Furthermore, microglia respond to BBB disruption events through
724 expression of inflammatory mediators plus debris removal to promote BBB restoration [55].
725 The upregulation of MHC I is part of this inflammatory response although it happens
726 regardless of BBB disruption [8, 13]. Interestingly, *in vivo* imaging experiments defined that
727 brain resident microglia migrate to the cerebral vasculature during systemic inflammation
728 [56]. We hypothesize that the upregulation of MHC class I molecules together with the
729 migration of microglia to areas that surround the cerebral vasculature might position

730 microglia at an optimal location for controlling CD8 T cell activation and further
731 exacerbating BBB disruption. Importantly, this modulation was also confirmed to be brain-
732 centered as observed by parabiosis experiments.

733 The mechanisms underlying microglial antigen presentation are still unknown.
734 Historically, the concept of cross-presentation has been restricted to dendritic cells which
735 engulf cellular debris and present processed peptides on MHC class I molecules to CD8
736 T cells [57]. However, it has also been reported that brain endothelial cells can cross-
737 present during Plasmodium berghei ANKA infection [58]. In this study, *in vitro* and *in vivo*
738 imaging methodology was employed to observe endothelial cell cross presentation of
739 OVA antigen [58]. This resulted in clear tracking of antigen processing and presentation in
740 culture and also the arrest of T cells engaging brain vasculature during acute infection [58].
741 Therefore, it is possible that additional NVU cell types can cross-present antigens. More
742 specifically, microglia could be engulfing cellular debris from TMEV infected neurons and
743 presenting viral antigen on MHC class I molecules to stimulate brain infiltrating CD8 T
744 cells. Additionally, in our study, the modulation of perforin expression on D^b:$VP2_{121-130}$
745 Tetramer+ CD8 T cells by MHC class I on microglia potentiates the BBB damage. It is
746 unclear whether this regulation would be beneficial in different disease models with
747 different degrees of BBB disruption.

748 Adaptive immune cell memory is an essential protective mechanism against recurring
749 infectious diseases. TMEV infection generates memory D^b:$VP2_{121-130}$ epitope specific
750 CD8 T cells which reside in the brain long after viral clearance [3]. Importantly, our data
751 demonstrates that the microglia H-$2D^b$ expression is not required for maintenance of
752 these memory CD8 T cells in the brain [3]. However, upon secondary encounter with the

753 immunodominant viral peptide $VP2_{121-130}$, ablation of H-$2D^b$ in microglia results in reduced
754 immune cell infiltration from the blood to the brain parenchyma. Although at first we did
755 not see a decrease in the numbers of D^b:$VP2_{121-130}$ Tetramer+ CD8 T cells in the
756 Tmem119 D^b cKO mice, when isolating the CD8 TRM response using FTY720 treatment,
757 we observed an important interaction between H-$2D^b$ expressing microglia and CD8 TRM
758 cells in the brain. This decreased expansion of CD8 TRM cells in Tmem119 D^b cKO mice
759 following $VP2_{121-130}$ injection was accompanied by attenuated BBB disruption visible by
760 MRI. This finding implies microglia antigen presentation enhances the CD8 TRM cell
761 response and overall immune cell infiltration, resulting in increased BBB permeability[3].
762 The fact that BBB permeability was not attenuated in Tmem119 D^b cKO without FTY720
763 treatment suggests that brain residing CD8 TRM cells can induce BBB regulation more
764 efficiently when additional infiltrating cell types are not present in brain parenchyma. This
765 form of regulation will be investigated in future studies. Nevertheless, our results are
766 highly relevant to our understanding of CD8 TRM function. Brain CD8 TRM cells have
767 been reported to be present in mouse models and human samples and may have a pivotal
768 role in the development and progression of neurological diseases [4, 5, 7, 59]. Our findings
769 demonstrate an important role for microglia class I restricted antigen presentation in
770 guiding these memory CD8 T cell populations.

771 The ability to enhance CD8 T cell responses through MHC class I-restricted antigen
772 presentation through discrete cell types may hold potential for therapeutic strategies in
773 diseases where CD8 T cells are known to play a pivotal role in neuropathology. Such
774 diseases include Cerebral Malaria, Multiple Sclerosis, Alzheimer's Disease and
775 Narcolepsy [34]. AAV-based therapies targeting discrete MHC class I molecules on

776 microglia could potentially control disease progression and severity. Although more
777 studies are needed to confirm the dynamics of these interactions in other disease models,
778 our results put forward microglia as a key antigen presenting cell in the context of MHC
779 class I during acute and memory phases of infectious disease, regulating CD8 T cell
780 proliferation and BBB integrity.

781 **Funding**

782 The authors received funding for this work through NIH Grants R01 NS103212, R01
783 NS122174, NIH training grant T32 AI170478 and the Center for MS and Autoimmune
784 Neurology at Mayo Clinic through the Eugene and Marcia Applebaum Fellowship.

785 **Acknowledgments**

786 We would like to thank the NIH tetramer core facility for providing tetramers that were
787 used in this work. Biorender.com was used to create the experimental design figures and
788 schematics.

789 **References**

790

791 1. Verma, A.K. & Perlman, S. Unraveling the complexities of neurotropic virus
792 infection and immune evasion. *Microbiol Mol Biol Rev* **89**, e0018523 (2025).

793
794 2. Ludlow, M. *et al.* Neurotropic virus infections as the cause of immediate and
795 delayed neuropathology. *Acta Neuropathol* **131**, 159-184 (2016).

796
797 3. Ayasoufi, K. *et al.* Brain resident memory T cells rapidly expand and initiate
798 neuroinflammatory responses following CNS viral infection. *Brain Behav Immun*
799 **112**, 51-76 (2023).

800
801 4. Kimura, K. *et al.* Resident Memory-like CD8(+) T Cells Are Involved in Chronic
802 Inflammatory and Neurodegenerative Diseases in the CNS. *Neurol Neuroimmunol*
803 *Neuroinflamm* **11** (2024).

5. Mix, M.R. *et al.* Repetitive antigen stimulation in the periphery dictates the composition and recall responses of brain-resident memory CD8(+) T cells. *Cell Rep* **44**, 115247 (2025).

6. Ning, J. *et al.* Functional virus-specific memory T cells survey glioblastoma. *Cancer Immunol Immunother* **71**, 1863-1875 (2022).

7. Musial, S.C. *et al.* Alarm Functions of PD-1+ Brain-Resident Memory T Cells. *J Immunol* **213**, 1585-1594 (2024).

8. Goddery, E.N. *et al.* Microglia and Perivascular Macrophages Act as Antigen Presenting Cells to Promote CD8 T Cell Infiltration of the Brain. *Front Immunol* **12**, 726421 (2021).

9. Syage, A. *et al.* Microglia influence immune responses and restrict neurologic disease in response to central nervous system infection by a neurotropic murine coronavirus. *Front Cell Neurosci* **17**, 1291255 (2023).

10. Zong, L. *et al.* Dual immune modulation of microglia in viral encephalitis: current understanding and future perspectives. *Front Mol Biosci* **12**, 1695058 (2025).

11. Zhang, Q., Sun, W., Zheng, M. & Zhang, N. Contribution of microglia/macrophage to the pathogenesis of TMEV infection in the central nervous system. *Front Microbiol* **15**, 1452390 (2024).

12. Bloomfield, C.L. *et al.* Retinal microglia express more MHC class I and promote greater T-cell-driven inflammation than brain microglia. *Front Immunol* **15**, 1399989 (2024).

13. Kellogg, C.M. *et al.* Microglial MHC-I induction with aging and Alzheimer's is conserved in mouse models and humans. *Geroscience* **45**, 3019-3043 (2023).

14. McGeer, P.L., Itagaki, S., Boyes, B.E. & McGeer, E.G. Reactive microglia are positive for HLA-DR in the substantia nigra of Parkinson's and Alzheimer's disease brains. *Neurology* **38**, 1285-1291 (1988).

15. Moseman, E.A., Blanchard, A.C., Nayak, D. & McGavern, D.B. T cell engagement of cross-presenting microglia protects the brain from a nasal virus infection. *Sci Immunol* **5** (2020).

16. McDole, J.R. *et al.* Rapid formation of extended processes and engagement of Theiler's virus-infected neurons by CNS-infiltrating CD8 T cells. *Am J Pathol* **177**, 1823-1833 (2010).

17. Mendez-Fernandez, Y.V., Johnson, A.J., Rodriguez, M. & Pease, L.R. Clearance of Theiler's virus infection depends on the ability to generate a CD8+ T cell response against a single immunodominant viral peptide. *Eur J Immunol* **33**, 2501-2510 (2003).

18. Johnson, A.J. *et al.* Prevalent class I-restricted T-cell response to the Theiler's virus epitope Db:VP2121-130 in the absence of endogenous CD4 help, tumor necrosis factor alpha, gamma interferon, perforin, or costimulation through CD28. *J Virol* **73**, 3702-3708 (1999).

19. Tritz, Z.P. *et al.* Conditional Silencing of H-2D(b) Class I Molecule Expression Modulates the Protective and Pathogenic Kinetics of Virus-Antigen-Specific CD8 T Cell Responses during Theiler's Virus Infection. *J Immunol* **205**, 1228-1238 (2020).

20. Claeys, W. *et al.* Limitations of PLX3397 as a microglial investigational tool: peripheral and off-target effects dictate the response to inflammation. *Front Immunol* **14**, 1283711 (2023).

21. Cao, K. *et al.* More than microglial depletion: PLX5622 activates the hepatic constitutive androstane receptor to alter anesthesia and addiction. *Neuron* (2026).

22. Meghraoui-Kheddar, A., Barthelemy, S., Boissonnas, A. & Combadiere, C. Revising CX3CR1 Expression on Murine Classical and Non-classical Monocytes. *Front Immunol* **11**, 1117 (2020).

23. Pavelko, K.D. *et al.* Theiler's murine encephalomyelitis virus as a vaccine candidate for immunotherapy. *PLoS One* **6**, e20217 (2011).

24. Willenbring, R.C. *et al.* Modulatory effects of perforin gene dosage on pathogen-associated blood-brain barrier (BBB) disruption. *J Neuroinflammation* **13**, 222 (2016).

25. Huggins, M.A. *et al.* Perforin Expression by CD8 T Cells Is Sufficient To Cause Fatal Brain Edema during Experimental Cerebral Malaria. *Infect Immun* **85** (2017).

885 26. Jung, S. *et al.* Analysis of fractalkine receptor CX(3)CR1 function by targeted
886 deletion and green fluorescent protein reporter gene insertion. *Mol Cell Biol* **20**,
887 4106-4114 (2000).

888
889 27. Kaiser, T. & Feng, G. Tmem119-EGFP and Tmem119-CreERT2 Transgenic Mice
890 for Labeling and Manipulating Microglia. *eNeuro* **6** (2019).

891
892 28. Faust, T.E. *et al.* A comparative analysis of microglial inducible Cre lines. *Cell Rep*
893 **42**, 113031 (2023).

894
895 29. Anani-Wolf, D.M. *et al.* Antigen-specific CD8 T cells are generated and reactivated
896 in the bone marrow following viral brain infections and impact the bone marrow
897 niche. *bioRxiv* (2025).

898
899 30. Borson, N.D. *et al.* Brain-infiltrating cytolytic T lymphocytes specific for Theiler's
900 virus recognize H2Db molecules complexed with a viral VP2 peptide lacking a
901 consensus anchor residue. *J Virol* **71**, 5244-5250 (1997).

902
903 31. Johnson, H.L. *et al.* Perforin competent CD8 T cells are sufficient to cause
904 immune-mediated blood-brain barrier disruption. *PLoS One* **9**, e111401 (2014).

905
906 32. Johnson, A.J. *et al.* Antigen-specific CD8+ T cells mediate a peptide-induced fatal
907 syndrome. *J Immunol* **174**, 6854-6862 (2005).

908
909 33. Suidan, G.L., McDole, J.R., Chen, Y., Pirko, I. & Johnson, A.J. Induction of blood
910 brain barrier tight junction protein alterations by CD8 T cells. *PLoS One* **3**, e3037
911 (2008).

912
913 34. Seady, M. & Johnson, A.J. CD8 T cells as drivers of blood-brain barrier disruption.
914 *Trends Neurosci* **48**, 483-494 (2025).

915
916 35. Lei, F. *et al.* CSF1R inhibition by a small-molecule inhibitor is not microglia specific;
917 affecting hematopoiesis and the function of macrophages. *Proc Natl Acad Sci U S*
918 *A* **117**, 23336-23338 (2020).

919
920 36. Harms, A.S. *et al.* MHCII is required for alpha-synuclein-induced activation of
921 microglia, CD4 T cell proliferation, and dopaminergic neurodegeneration. *J*
922 *Neurosci* **33**, 9592-9600 (2013).

923

924 37. Wolf, Y. *et al.* Microglial MHC class II is dispensable for experimental autoimmune
925 encephalomyelitis and cuprizone-induced demyelination. *Eur J Immunol* **48**, 1308-
926 1318 (2018).

927
928 38. Schetters, S.T.T., Gomez-Nicola, D., Garcia-Vallejo, J.J. & Van Kooyk, Y.
929 Neuroinflammation: Microglia and T Cells Get Ready to Tango. *Front Immunol* **8**,
930 1905 (2017).

931
932 39. Rothenberg, B.E. & Voland, J.R. beta2 knockout mice develop parenchymal iron
933 overload: A putative role for class I genes of the major histocompatibility complex
934 in iron metabolism. *Proc Natl Acad Sci U S A* **93**, 1529-1534 (1996).

935
936 40. Praetor, A. & Hunziker, W. beta(2)-Microglobulin is important for cell surface
937 expression and pH-dependent IgG binding of human FcRn. *J Cell Sci* **115**, 2389-
938 2397 (2002).

939
940 41. Groh, V., Steinle, A., Bauer, S. & Spies, T. Recognition of stress-induced MHC
941 molecules by intestinal epithelial gammadelta T cells. *Science* **279**, 1737-1740
942 (1998).

943
944 42. Robinson, P.J., Travers, P.J., Stackpoole, A., Flaherty, L. & Djaballah, H.
945 Maturation of Qa-1b class I molecules requires beta 2-microglobulin but is TAP
946 independent. *J Immunol* **160**, 3217-3224 (1998).

947
948 43. Yamaguchi, H. & Hashimoto, K. Association of MR1 protein, an MHC class I-
949 related molecule, with beta(2)-microglobulin. *Biochem Biophys Res Commun* **290**,
950 722-729 (2002).

951
952 44. Yokoyama, K., Stockert, E., Old, L.J. & Nathenson, S.G. Structural evidence that
953 the small subunit found associated with the TL antigen is beta 2-microglobulin.
954 *Immunogenetics* **15**, 543-549 (1982).

955
956 45. Bauer, A. *et al.* Analysis of the requirement for beta 2-microglobulin for expression
957 and formation of human CD1 antigens. *Eur J Immunol* **27**, 1366-1373 (1997).

958
959 46. Santos, M. *et al.* Defective iron homeostasis in beta 2-microglobulin knockout mice
960 recapitulates hereditary hemochromatosis in man. *J Exp Med* **184**, 1975-1985
961 (1996).

962
963 47. Wang, Q.L. *et al.* Association of HLA diversity with the risk of 25 cancers in the UK
964 Biobank. *EBioMedicine* **92**, 104588 (2023).

48. Fain, C.E. *et al.* Discrete class I molecules on brain endothelium differentially regulate neuropathology in experimental cerebral malaria. *Brain* **147**, 566-589 (2024).

49. Hill, A.V. *et al.* Common west African HLA antigens are associated with protection from severe malaria. *Nature* **352**, 595-600 (1991).

50. Lin, M. *et al.* Association of HLA class I with severe acute respiratory syndrome coronavirus infection. *BMC Med Genet* **4**, 9 (2003).

51. Naruto, T. *et al.* Selection of HLA-B57-associated Gag A146P mutant by HLA-B *48:01-restricted Gag140-147-specific CTLs in chronically HIV-1-infected Japanese. *Microbes Infect* **13**, 766-770 (2011).

52. Mayer, M.G. & Fischer, T. Microglia at the blood brain barrier in health and disease. *Front Cell Neurosci* **18**, 1360195 (2024).

53. Ronaldson, P.T. & Davis, T.P. Regulation of blood-brain barrier integrity by microglia in health and disease: A therapeutic opportunity. *J Cereb Blood Flow Metab* **40**, S6-S24 (2020).

54. Knopp, R.C., Banks, W.A. & Erickson, M.A. Physical associations of microglia and the vascular blood-brain barrier and their importance in development, health, and disease. *Curr Opin Neurobiol* **77**, 102648 (2022).

55. Nguyen, R.H. *et al.* Imaging a concussion and the ensuing immune response at the blood-brain barrier. *Proc Natl Acad Sci U S A* **122**, e2414316122 (2025).

56. Haruwaka, K. *et al.* Dual microglia effects on blood brain barrier permeability induced by systemic inflammation. *Nat Commun* **10**, 5816 (2019).

57. Kurts, C., Robinson, B.W. & Knolle, P.A. Cross-priming in health and disease. *Nat Rev Immunol* **10**, 403-414 (2010).

58. Aydin, S. *et al.* Antigen recognition detains CD8(+) T cells at the blood-brain barrier and contributes to its breakdown. *Nat Commun* **14**, 3106 (2023).

59. Smolders, J. *et al.* Tissue-resident memory T cells populate the human brain. *Nat Commun* **9**, 4593 (2018).

Supplementary Files

This is a list of supplementary files associated with this preprint. Click to download.

- Supplementaryfigures.docx